Journal of Computational Physics **172,** 119–165 (2001)
doi:10.1006/jcph.2001.6817, available online at http://www.idealibrary.com on IDEAL®

A Novel Velocity–Vorticity Formulation of the Navier–Stokes Equations with Applications to Boundary Layer Disturbance Evolution

Christopher Davies* and Peter W. Carpenter†

**School of Mathematical and Information Sciences, Coventry University, Priory Street, Coventry CV1 5FB, United Kingdom; and †School of Engineering, University of Warwick, Coventry CV4 7AL, United Kingdom*
E-mail: cdavies@coventry.ac.uk

Received November 27, 2000; revised April 23, 2001

A novel velocity–vorticity formulation of the unsteady, three-dimensional, Navier–Stokes equations is presented. The formulation is particularly suitable for simulating the evolution of three-dimensional disturbances in boundary layers. A key advantage is that there are only *three* governing equations for three primary dependent variables. Another advantage is that no wall boundary conditions are needed for the vorticity. Instead the conditions placed on the velocity are linked to the vorticity field through integral constraints based on the definition of vorticity.

Numerical methods are presented in the context of application to the three-dimensional boundary layer over a rotating disc. The discretization scheme uses spectral expansions in the wall-normal and azimuthal (or spanwise) directions and compact finite differences in the radial (or streamwise) direction. The scheme is implemented so that the advantages of spectral convergence can be combined with the use of an efficient line-iteration solution procedure. The linearized form of the new velocity–vorticity method is validated for the case of convective instabilities evolving over both rigid and compliant discs.

1. INTRODUCTION

Velocity–vorticity methods have many attractive features as a basis for calculating unsteady flow fields. Accordingly, it is all the more unfortunate that the methods currently in use generally suffer from two major drawbacks. Firstly, for unsteady three-dimensional problems they require six dependent variables which compares poorly with the four required in formulations using primitive variables. Secondly, the lack of a boundary condition on vorticity can make it necessary to adopt relatively elaborate schemes in order to ensure that the computed velocity and vorticity fields are divergence-free. We will show that both of these drawbacks can be overcome for an important class of problems.

0021-9991/01 $35.00

Our novel formulation stems from a desire to develop an efficient, yet versatile, method for simulating the evolution of three-dimensional perturbations in boundary layers. We are particularly interested in simulating passive and active flow control; for example, the use of finite-length compliant panels [14] and MEMS and micro actuators in the form of deformable bumps or jets issuing from orifices in the wall [8, 9, 11, 32, 33, 50]. These are highly elliptic problems featuring rapid change in the streamwise direction and also local upstream propagation of disturbances. This latter feature is also found when there are absolute instabilities. We wished to develop a computational method that could be used for full direct numerical simulations but, at the same time, would also be suitable for integrating the linearized Navier–Stokes equations. In this respect it would emulate the PSE (Parabolic Stability Equation) approach developed by Bertolotti *et al.* [4] (see, also, [31]). However, unlike the PSE approach, our method is fully elliptic and no restrictions are placed on the form of the disturbance. We do not, however, expect our method to compete in terms of computational efficiency for problems which are suitable for using the PSE approach. That said, we can see no reason why our velocity–vorticity formulation could not be used as the basis of a three-dimensional PSE scheme.

Fasel [22], Speziale [57], and Gatski [25] review the advantages of velocity–vorticity methods. One of the main advantages is the elimination of the pressure by using the Navier–Stokes equations in the form of a vorticity transport equation

$$\frac{D\boldsymbol{\Omega}}{Dt} = \boldsymbol{\Omega} \cdot \nabla \mathbf{U} + \nu \nabla^2 \boldsymbol{\Omega}, \tag{1}$$

where D/Dt denotes the material derivative, $\boldsymbol{\Omega}$ and $\mathbf{U}$ denote, respectively, the three-dimensional vorticity and velocity vector fields, and ν is the kinematic viscosity. Thus, only three dependent variables need to be updated in time, as compared with four when using primitive variables. Equation (1) is supplemented by the continuity equation and the definition of vorticity, i.e.,

$$\nabla \cdot \mathbf{U} = 0, \quad \boldsymbol{\Omega} = \nabla \times \mathbf{U}. \tag{2a,b}$$

Here Eq. (2a) is written in the form used for incompresssible flow. In principle, Eqs. (1), (2a) and (2b) are sufficient for determining the velocity and vorticity fields. However, many velocity–vorticity methods use a Poisson equation, obtained by taking the curl of Eq. (2b) and making use of (2a) to determine the velocity from the vorticity. This Poisson equation takes the form:

$$\nabla^2 \mathbf{U} = -\nabla \times \boldsymbol{\Omega}. \tag{3}$$

Gatski [25] classified velocity–vorticity methods proper into two basic categories, both of which use the vorticity transport equation (1) to update the vorticity but differ in how the velocity is then subsequently determined from the vorticity field: (1) *Method A* solves Eqs. (2a) and (2b) sequentially or simultaneously for **U**—examples include the studies made by Gatski *et al.* [26, 27], Koh and Bradshaw [41], and Bertagnolio and Daube [3]; and (2) *Method B* solves the Poisson equation (3) for **U**—examples include the works of Fasel [21, 22], Dennis and Quartapelle [20], Fasel and Konzelmann [23], Fasel *et al.* [24], Kral and Fasel [42], Kloker *et al.* [39], Rempfer and Fasel [52, 53], Rist and Fasel [54], Wu, Wu, and Wu [61], Trujillo and Karniadakis [59], and Meitz and Fasel [49].

As mentioned above, difficulties can arise with velocity–vorticity methods, in ensuring that both Eqs. (2a) and (2b) are properly satisfied by the numerical solution. For example, in the case of Method B, although Eq. (2a) is used to obtain Eq. (3), a divergence-free velocity field is not necessarily guaranteed. However, it can be shown [22] that provided Eq. (2a) is satisfied on the boundary of the computational domain, it will be satisfied in the interior (in practice this implies that the error is maximal on the boundary). It can also be shown that provided the computed vorticity field is solenoidal, the velocity field computed using Eq. (3) will satisfy Eq. (2b) everywhere in the domain, provided that Eq. (2b) is satisfied on the boundary. These considerations led Fasel and his coworkers to formulate numerical boundary conditions in terms of the first and second derivatives of the perturbation vorticity components. This approach usually works well in practice, but, as will be discussed in more detail below, it can lead to difficulties in the case of parallel or near-parallel undisturbed flows.

Gresho [28, 29] and more recently Weinan and Liu [60] critically review and analyze the various forms of the vorticity boundary condition used by previous authors. A common view has developed over the past ten years or so that any vorticity boundary condition has to be global in the sense that the values at all points on the boundary should be linked. However, Weinan and Liu show that in the context of finite-difference schemes, at least, many of the newly developed global boundary conditions are actually equivalent to older local formulae. They thereby cast serious doubt on the usefulness of these global boundary conditions since they are much more complicated to implement than local ones. Our view, as will be seen, is that an integral constraint is a far more satisfactory and simpler, truly global, alternative to a boundary condition.

Many authors (e.g., Gatski *et al.* [26, 27], Wu, Wu, and Wu [61] and Bertagnolio and Daube [3]) decompose their computed vorticity field $\boldsymbol{\Omega}^c$, which is not divergence-free in general, into a solenoidal $\nabla\phi$ and rotational part $\boldsymbol{\Omega}$. It therefore follows that

$$\nabla^2\phi = \nabla \cdot \boldsymbol{\Omega}^c. \tag{4}$$

Equation (4) can then be solved for $\nabla\phi$ which is used to project the computed $\boldsymbol{\Omega}^c$ field onto a divergence-free field,

$$\boldsymbol{\Omega} = \boldsymbol{\Omega}^c - \nabla\phi. \tag{5}$$

Wu, Wu, and Wu [61] established the conditions for optimum projection and also showed that it is possible to solve Eq. (3) for a divergence-free velocity field using an *arbitrary* non-solenoidal $\boldsymbol{\Omega}^c$ in place of $\boldsymbol{\Omega}$. They showed that the projection can be carried out relatively cheaply without the need for a time-consuming inversion of a Poisson equation. Recently, Bertagnolio and Daube [3] generalized this approach of a Helmholtz decomposition combined with projection onto a space of divergence-free vectors to generalized curvilinear coordinates.

In any discussion of vorticity boundary conditions, it is important to appreciate that the only fundamental boundary conditions are those that must be imposed on the velocity field. (See [28, 29] for a detailed discussion of this point.) When boundary conditions on the vorticity are derived and utilized within a particular formulation of the Navier–Stokes equations, they cannot provide any constraints that are genuinely additional to those that are required for the velocity. For instance, in the velocity–vorticity formulation adopted by Fasel

et al. [24] the conditions imposed on the velocity field provide the boundary conditions for Poisson-type equations that relate the velocity field to the vorticity field. Exactly the same information is employed, a second time, to obtain boundary conditions for the vorticity. These latter conditions are derived by simply substituting the boundary conditions imposed on the velocity field into algebraic relations that follow from the Poisson equations, the vorticity definition, and the continuity equation.

Because there is no general requirement to impose any constraint on the vorticity that cannot be traced back to the conditions imposed on the velocity field, the apparent necessity for vorticity boundary conditions is often an artifice of the chosen numerical method. Indeed, as pointed out by Gresho, nearly thirty years ago Davis [17] formulated a streamfunction–vorticity method based on finite differences that implicitly discarded the need for any boundary conditions on vorticity. A little later, Barrett [2] and Campion–Renson and Crochet [7] independently also proposed streamfunction–vorticity methods, this time based on finite elements, in which no boundary condition is imposed on vorticity. In effect, in such schemes the vorticity is constrained or determined by some sort of integral relation, or its equivalent, over the computational domain which relates the unknown value of the vorticity at the boundary to its values in the interior without any need to specify the former. An approach of this kind has been proposed by Dennis and Quartapelle [20] who use Green's theorem to generate a set of integral conditions of this sort. Dennis and Hudson [18, 19] propose a hybrid of Gatski's Methods A and B which for two-dimensional flows solves one of the Poisson equations (3) for one of the velocity components and then integrate the continuity equation to solve for the other. Shen and Loc [56] have proposed a three-dimensional version of this approach.

Perhaps the most straightforward example of the use of an integral constraint on vorticity is provided by Guevremont *et al.* [30]. They impose no boundary conditions on vorticity in their two-dimensional finite-element method. Instead, a weighted integral relation is imposed which is based on the definition of vorticity and evaluated over the entire domain. Our approach bears some similarity to that of Guevremont *et al.*, although it was developed in ignorance of their work. It is a hybrid of Methods A and B. We solve the Poisson equation (3) for the normal velocity component and use the definition of vorticity (2b) to link the surface values of the other two velocity components to integrals of the vorticity components. The two-dimensional version was given by Davies and Carpenter [14]. Thus, this method replaces boundary conditions with integral conditions on vorticity which link it to the boundary conditions on velocity on the solid surface in a natural and very straightforward way. In many cases, of course, it is simply the no-slip condition that is imposed on the solid surface. This approach provides a relatively simple, but rigorous, method for ensuring a divergence-free velocity field and finding a solution to the vorticity field that satisfies Eq. (2b).

We will now discuss the principal disadvantage of the current three-dimensional velocity–vorticity methods, namely that it appears to be necessary to solve the three transport equations (1) for the vorticity components, as well as the three Poisson equations (3), or their equivalents, for the velocity components. In contrast, for two dimensions the velocity–vorticity formulation can readily be reduced to two governing equations. An obvious way to achieve this is to use a streamfunction–vorticity formulation such as, for example, Dennis and Quartapelle [20]. It is also possible to retain the velocity–vorticity formulation and eliminate the streamwise velocity component between the continuity equation (2a) and the definition of vorticity (2b). This approach was followed independently by Koh and Bradshaw

[41] and Davies and Carpenter [14]. Wu, Wu and Wu [61] point out that in three dimensions the continuity equation (2a) can be used to determine the third component of velocity rather than solving a third Poisson equation. Adopting this procedure can lead to considerable savings in CPU time, especially if projection onto a divergence-free space is required. Nevertheless, our intuition suggested that it should be possible to carry out three-dimensional calculations with only *three* (primary) governing equations. And, indeed, in the present paper we show how it is possible for a wide class of problems to derive a velocity–vorticity formulation which is based on only three *primary* dependent variables.

In fact, Kim, Moin, and Moser [37] have already shown that for homogeneous flow in a planar channel, at least, it is feasible to employ a velocity–vorticity formulation that involves only two primary dependent variables and two evolution equations. One evolution equation determines the Laplacian of the normal velocity component, while the other is just the usual transport equation for the normal component of the vorticity. The remaining two velocity components are obtained by applying the continuity equation and the definition of the normal component of the vorticity. For the doubly spatially periodic computational domain appropriate to homogeneous channel flow, the construction of the spanwise and streamwise components of the velocity from the normal components of the velocity and the vorticity may be accomplished in a direct and efficient manner, using relatively simple manipulations of Fourier series representations for the flow-variables. However, it is not obvious that a similarly efficient numerical method could be implemented for more general flow configurations that are not periodic along two spatial directions, or geometrically simple in some other fashion.

A distinctive, but potentially disadvantageous, feature of the formulation adopted by Kim, Moin, and Moser is that it involves a fourth-order evolution equation for the normal velocity component. This apparent drawback was successfully dealt with by introducing an intermediate variable within a numerical scheme that split the fourth-order equation into a pair of coupled second-order equations. The first of these split equations may be classified as a vorticity-type transport equation, while the second takes the simpler form of a Poisson equation. Thus, the system of governing equations used by Kim, Moin, and Moser consisted, in practice, of two vorticity-type transport equations and a single Poisson equation. We shall develop a velocity–vorticity formulation that involves a similar system of governing equations. However, our formulation would appear to be less restrictive with regard to the flow and the bounding surface geometry. Moreover, the ease of its numerical implementation is not fine-tuned to any presumed streamwise periodicity of the computational domain. We shall show, in particular, that our velocity–vorticity formulation readily lends itself to the efficient simulation of disturbances in spatially inhomogeneous flows.

In our standard formulation, the dependent variables are perturbations, which are finite in general, to a known undisturbed flow field. The geometry is relatively simple, as illustrated in Fig. 1. We envisage a three-dimensional flow field over a flat or slightly curved solid surface. The solid surface need not be completely rigid. Part of it may be replaced by a compliant surface or some other sort of interactive device, such as a suction hole or slot, or a microjet-type actuator.

The three primary dependent variables are the two perturbation vorticity components in the plane of the solid surface and the perturbation normal velocity component. These are governed by two vorticity transport equations and a Poisson equation. The secondary dependent variables are the remaining vorticity and velocity components and pressure. The distinction between primary and secondary dependent variables is that the latter can

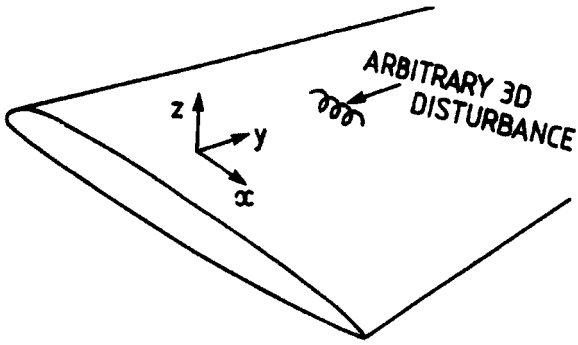

FIG. 1. Arbitary three-dimensional disturbance in a three-dimensional flow over a solid surface.

be determined explicitly entirely from the current values of the former. Accordingly, the secondary variables can, in principle, be eliminated from consideration and storage is not required for them. We will show that, provided the dependent variables can be forced to satisfy certain rather general conditions at infinity, this formulation is fully equivalent to the Navier–Stokes equations in primitive-variable form.

Owing to our interest in simulating the evolution of perturbations in boundary layers, the velocity–vorticity approach of Fasel and his coworkers, was an attractive starting point. In many respects, despite the evident differences, our method can be regarded as a natural development from theirs. It is obviously computationally more advantageous to work with only three primary governing equations. A further, less-evident advantage of our formulation is that it allows spectral discretization in the normal, as well as the spanwise, directions. Finite differences are used only for the streamwise direction. Furthermore, it is possible to retain simple pentadiagonal and tridiagonal matrix schemes even with our spectral discretization. This feature leads to additional computational efficiency.

The present paper is mostly devoted to describing the formulation and other theoretical and numerical aspects of our velocity–vorticity method. But we also provide evidence of its practical utility by describing a numerical study of the convective instabilities of the three-dimensional boundary layer over a rotating disc. The study includes cases where a compliant annulus is inset into the disc's surface. For this particular application, we consider small-amplitude disturbances and employ a linearized form of the governing equations. An overview of the literature on the rotating disc boundary layer is given in the reviews by Reed and Saric [51] and Cooper and Carpenter [12]. Here we will only provide a minimal account that is sufficient to motivate our numerical study.

The standard linear stability analysis for the rotating disc boundary layer is based on a sixth-order system of ordinary differential equations [46, 48]. The results of this analysis are well-documented and can be used to provide validation for our computer code. However, the standard stability analysis neglects the slow variation of the flow variables in the radial direction. Our method, being based on the complete linearized governing equations, does not need to make any such assumption. Accordingly, we can study the effects of including the so-called "nonparallel terms." It turns out that they have only a slight effect on the convective instabilities. This is in accord with the results of an earlier study by Malik and Balakumar [47] using the PSE approach.

Three distinct families of eigenmodes have been identified for the rotating-disc boundary layer. Recently Lingwood [43, 44] showed that the Type I mode (which is essentially an

inviscid inflexion-point instability) coalesces with the, hitherto obscure, Type III mode to form an absolute instability. She also noted that the Types I and II modes could coalesce. (The Type II is a viscous mode and is destabilized by the effects of Coriolis acceleration.) In this case, the coalescence first occurs when the individual eigenmodes are convectively stable. Koch [40] suggested that, since such a coalescence, which he termed direct resonance, corresponds to a double root, the Cauchy residue theorem could be used to evaluate the form of the coalesced mode. He thereby showed that algebraic growth would occur. For sufficiently high levels of background noise, algebraic growth could provide a route to transition. Our numerical simulations were successful in confirming the existence of the algebraic growth, thus providing a particularly stringent validation of the computer code. However, in this instance the effects of the so-called "nonparallel" terms were found to be much more significant. The "nonparallel" simulations suggest that, in practice, for a rigid disc the algebraic growth would be dominated by the onset of convective instability slightly further outboard.

A separate paper will be devoted to a study of the implications of the absolute instability for global behavior. It suffices here to note that such a study has, in fact, been successfully undertaken [16] using our new velocity–vorticity formulation and discretization scheme to conduct an appropriate set of numerical simulations in an efficient manner. The results of these simulations appear to suggest that the slow radial flow variation does have an important effect, which leads to a qualitative change in the global behavior of the rotating-disc boundary layer, compared with Lingwood's [43] local "parallel-flow" theory.

The remainder of the present paper is set out as follows. Section 2 describes our velocity–vorticity formulation of the Navier–Stokes equations for the general case. In Section 3, we adapt the formulation for the rotating-disc flow. The numerical methods are described in Section 4. The results of a study of the convective instabilities of the rotating-disc boundary layer obtained with our velocity–vorticity method are presented and discussed in Section 5. Finally, the conclusions are given in Section 6.

2. REFORMULATION OF THE NAVIER–STOKES EQUATIONS

In this section we describe the new velocity–vorticity formulation of the Navier–Stokes equations and demonstrate its equivalence to the usual formulation in terms of primitive variables. We suppose that there is an incompressible fluid flow in the semi-infinite domain $z \in [\eta, \infty)$, where $z = \eta(x, y, t)$ defines the location of a solid, but possibly nonstationary or porous boundary to the flow domain. For the case where the boundary is a flat rigid wall, we will set $\eta = 0$. Consequently, z will be referred to as the wall-normal coordinate. It is assumed that there is a known undisturbed-flow solution represented by the velocity and vorticity fields

$$\mathbf{U}^B = (U^B, V^B, W^B), \quad \boldsymbol{\Omega}^B = \left(\Omega_x^B, \Omega_y^B, \Omega_z^B\right).$$

The total velocity and vorticity fields are then decomposed as

$$\mathbf{U} = \mathbf{U}^B + \mathbf{u}, \quad \boldsymbol{\Omega} = \boldsymbol{\Omega}^B + \boldsymbol{\omega}, \tag{6a,b}$$

where

$$\mathbf{u} = (u, v, w), \quad \boldsymbol{\omega} = (\omega_x, \omega_y, \omega_z)$$

represent perturbations from the prescribed undisturbed flow. We will consider the governing equations for perturbations rather than the total flow-variables, since this yields a more convenient formulation for present purposes. (If so desired, the undisturbed flow can be determined by making slight modifications to the governing equations for the perturbations. Details are included Appendix A, together with some comments about how the formulation could be amended when there is an upper physical boundary located at finite z.) The assumption of a Cartesian coordinate system provides for an economic exposition, but is not essential. Cylindrical polar coordinates will be employed for the rotating-disc problem.

We first divide the components of the perturbation flow-fields $\boldsymbol{u}, \boldsymbol{\omega}$ into two sets. The components $\{\omega_x, \omega_y, w\}$ will be referred to as *primary variables* while the remaining components $\{u, v, \omega_z\}$ will be identified as *secondary* variables. The primary variables are obtained by projecting the velocity field along the wall-normal direction and projecting the vorticity field on to the orthogonal plane, which is parallel to the wall. The order of combination of these projections with the velocity and vorticity fields is reversed in the case of the secondary variables. The distinction between primary and secondary variables is made because the latter may be defined explicitly in terms of the former, and thus, in principle, eliminated completely from consideration.

From this point on, unless explicitly stated otherwise, all variables will be dimensionless. We will show that the evolution of the three dimensionless primary variables $\{\omega_x, \omega_y, w\}$ may be determined using just three equations, namely

$$\frac{\partial \omega_x}{\partial t} + \frac{\partial N_z}{\partial y} - \frac{\partial N_y}{\partial z} = \frac{1}{R}\nabla^2 \omega_x \tag{7}$$

$$\frac{\partial \omega_y}{\partial t} + \frac{\partial N_x}{\partial z} - \frac{\partial N_z}{\partial x} = \frac{1}{R}\nabla^2 \omega_y \tag{8}$$

$$\nabla^2 w = \frac{\partial \omega_x}{\partial y} - \frac{\partial \omega_y}{\partial x}, \tag{9}$$

where $\mathbf{N} = (N_x, N_y, N_z)$ is defined as

$$\mathbf{N} = \boldsymbol{\Omega}^B \times \boldsymbol{u} + \boldsymbol{\omega} \times \boldsymbol{U}^B + \boldsymbol{\omega} \times \boldsymbol{u}. \tag{10}$$

The Reynolds number R is defined in the usual manner, using the appropriate velocity and length scales chosen for the nondimensionalization. The two equations (7) and (8) are the transport equations for the x and y components of the vorticity. The form for $\mathbf{N}$ shows that the full nonlinearity of the transport equations has been retained. For the rotating-disc numerical simulations, a linearization was performed by dropping the final term in Eq. (10). It should be stressed that the linearization, useful though it is for studies of the evolution of small-amplitude disturbances, is not an inherent feature of our velocity–vorticity formulation. Equation (9) can be obtained by taking the wall-normal component of the relationship

$$\nabla^2 \boldsymbol{u} = -\nabla \times \boldsymbol{\omega},$$

which is the perturbation form of Eq. (3).

Clearly, the convective quantity $\boldsymbol{N}$ appearing in the transport equations can only be fully evaluated if the secondary variables $\{u, v, \omega_z\}$ are known. Accordingly we make the explicit

definitions

$$u = -\int_z^\infty \left(\omega_y + \frac{\partial w}{\partial x}\right) dz \tag{12}$$

$$v = \int_z^\infty \left(\omega_x - \frac{\partial w}{\partial y}\right) dz \tag{13}$$

$$\omega_z = \int_z^\infty \left(\frac{\partial \omega_x}{\partial x} + \frac{\partial \omega_y}{\partial y}\right) dz. \tag{14}$$

The first two of these definitions can be obtained by integrating the appropriate components of the definition (2b) of vorticity with respect to z. It is assumed that both u and v vanish at infinity. The definition of ω_z follows from integration of the condition that the vorticity be solenoidal. With the definitions (12)–(14) of the secondary variables, the quantity $\boldsymbol{N}$ can be written explicitly in terms of the primary variables. The two transport equations (7) and (8), together with the Poisson equation (9), can thus be viewed as a system of three governing equations for the three unknown primary variables; all reference to the secondary variables may be eliminated.

Thus far, we have indicated how three differential equations and three explicit definitions can be derived for the six components of the velocity and vorticity perturbation fields. We now show that, from such a limited basis, it is possible to recover the full Navier–Stokes equations in primitive-variables form, provided two further conditions are satisfied for the behavior of the perturbations as $z \to \infty$.

2.1. *Equivalence to the Primitive Variables Formulation*

Differentiating Eqs. (12) and (13) with respect to z we obtain the relations:

$$\omega_x = \frac{\partial w}{\partial y} - \frac{\partial v}{\partial z}, \quad \omega_y = \frac{\partial u}{\partial z} - \frac{\partial w}{\partial x}. \tag{15a,b}$$

Substituting Eqs. (15a) and (15b) into Eq. (14) and carrying out the integration gives

$$\omega_z = \frac{\partial v}{\partial x} - \frac{\partial u}{\partial y}. \tag{16}$$

Thus, the secondary variables $\{u, v, \omega_z\}$ are defined so that the vorticity does, in fact, satisfy the usual definition (2b) of vorticity. The solenoidal property of the vorticity perturbation field

$$\nabla \cdot \boldsymbol{\omega} = 0.$$

follows immediately. (It also follows automatically from the definition of the secondary variable ω_z given in Eq. (14).)

If we differentiate the definition (12) of u with respect to x, the definition (13) of v with respect to y and then add we obtain

$$\frac{\partial u}{\partial x} + \frac{\partial v}{\partial y} = -\int_z^\infty \left(\frac{\partial \omega_y}{\partial x} - \frac{\partial \omega_x}{\partial y} + \frac{\partial^2 w}{\partial x^2} + \frac{\partial^2 w}{\partial y^2}\right) dz. \tag{17}$$

Substituting for the integrand using the Poisson equation (9) then gives

$$\frac{\partial u}{\partial x} + \frac{\partial v}{\partial y} + \frac{\partial w}{\partial z} = \lim_{z\to\infty} \frac{\partial w}{\partial z}. \tag{18}$$

It follows therefore that we can recover the incompressibility condition (2a), provided that

$$\lim_{z\to\infty} \frac{\partial w}{\partial z} = 0. \tag{19}$$

This does not represent an additional constraint so far as the primitive-variables formulation of the Navier–Stokes equations is concerned. It is satisfied automatically if incompressibility is enforced and the u, v components of the perturbation velocity vanish as $z \to \infty$. However, in our formulation, it would appear that the condition (19) needs to be imposed directly. We will show that, in practice, this presents no difficulty, provided an appropriate coordinate transformation is utilized to map the physically semi-infinite domain in the z-direction on to a finite computational domain.

Differentiating the vorticity transport equations (7) and (8) with respect to x, y, respectively, adding the results, and then using the solenoidal property of the perturbation vorticity field gives

$$\frac{\partial}{\partial z}\left(\frac{\partial \omega_z}{\partial t} + \frac{\partial N_y}{\partial x} - \frac{\partial N_x}{\partial y}\right) = \frac{\partial}{\partial z}\left(\frac{1}{R}\nabla^2\omega_z\right). \tag{20}$$

By integrating this with respect to z it may be concluded that the transport equation for ω_z will hold at all z-locations if it can be satisfied in the limit as $z \to \infty$. Thus, we can recover the transport equation

$$\frac{\partial \omega_z}{\partial t} + \frac{\partial N_y}{\partial x} - \frac{\partial N_x}{\partial y} = \frac{1}{R}\nabla^2\omega_z, \tag{21}$$

provided the perturbation flow-fields can be determined in a manner that ensures

$$\lim_{z\to\infty}\left\{\frac{\partial \omega_z}{\partial t} + \frac{\partial N_y}{\partial x} - \frac{\partial N_x}{\partial y} - \frac{1}{R}\nabla^2\omega_z\right\} = 0. \tag{22}$$

The secondary variables $\{u, v, \omega_z\}$ are all defined so as to vanish in the limit as the wall-normal coordinate approaches infinity. We will also assume that the velocity perturbation component w vanishes and that the corresponding component W^B of the undisturbed flow tends to a constant. (This constant will be zero for many boundary-layer flows, for example the flow over a flat plate, but is nonzero for the von-Kármán flow over a rotating disc.) The condition (22) may then be simplified to

$$\lim_{z\to\infty}\left(-W^B + \frac{1}{R}\frac{\partial}{\partial z}\right)\left(\frac{\partial \omega_x}{\partial x} + \frac{\partial \omega_y}{\partial y}\right) = 0, \tag{23}$$

where the solenoidal property of the vorticity has been reapplied to obtain a condition in terms of primary variables only. Such a condition would automatically be satisfied for the vorticity components ω_x, ω_y that could be derived from solutions of the Navier–Stokes equations in the usual primitive variables formulation. In our formulation it would appear

to be necessary to impose (23) directly. However, as with the previous condition (19) required for ensuring incompressibility, the need for any explicit enforcement of (23) can be circumvented by making a judicious choice of coordinate mapping in the z-direction. More details will be given later.

Assuming that some means is found for satisfying condition (23), the vorticity transport equation (21) for the component ω_z can be combined with the vorticity transport equations (7) and (8) for the other two components ω_x, ω_y to give

$$\nabla \times \left\{ \frac{\partial \boldsymbol{u}}{\partial t} + \boldsymbol{U}^B \cdot \nabla \boldsymbol{u} + \boldsymbol{u} \cdot \nabla \boldsymbol{U}^B + \boldsymbol{u} \cdot \nabla \boldsymbol{u} - \frac{1}{R} \nabla^2 \boldsymbol{u} \right\} = 0, \tag{24}$$

where the definition (2b) of vorticity has been used to eliminate any direct reference to the perturbation vorticity field and there has been some straightforward manipulation using vector identities. (Note that definition 2b is not assumed *a priori*, but is shown above to follow from our formulation.) Since we are dealing with the simply connected domain defined by $z \geq \eta(x, y, t)$, the irrotational vector quantity which appears enclosed in brackets in (24) may be written as the gradient of some scalar field. This scalar field can be identified as the negative of the perturbation pressure field. Hence, we can recover the momentum equations for the perturbation velocity components in the usual primitive-variables form.

We have now shown that the primitive-variables formulation of the Navier–Stokes equations can be obtained from our compact velocity–vorticity formulation. It should be recalled that the latter formulation comprises the three governing equations (7), (8), and (9) for the primary variables $\{\omega_x, \omega_y, w\}$ together with the relations (12)–(14) which define the secondary variables $\{u, v, \omega_z\}$. Full equivalence can only be ensured if the primary variables are constrained to satisfy the limiting conditions (19) and (23). The assumption was also made that all three components of the perturbation velocity field vanish for $z \to \infty$. Such behavior was built into the definitions of the secondary variables u, v. By contrast, the vanishing of w may be used to provide a boundary condition for the solution of the Poisson equation (9). We will now discuss what other boundary conditions must be imposed, and how they can be associated, individually, with each of the governing equations for the primary variables.

2.2. *Velocity Boundary Conditions at the Wall*

The motion of the fluid must be matched to that of the solid wall which is located at $z = \eta(x, y, t)$. This gives boundary conditions of the general form

$$u(x, y, \eta, t) = u_w(x, y, t), \tag{25}$$

$$v(x, y, \eta, t) = v_w(x, y, t), \tag{26}$$

$$w(x, y, \eta, t) = w_w(x, y, t), \tag{27}$$

where u_w, v_w, w_w are functions determined by the wall motion or otherwise. For example, if the fluid was bounded by a flexible wall which could only move in the z-direction we would need to set

$$u_w(x, y, t) = -U^B(x, y, \eta, t), \tag{28}$$

$$v_w(x, y, t) = -V^B(x, y, \eta, t), \tag{29}$$

$$w_w(x, y, t) = \frac{\partial \eta}{\partial t}(x, y, t) - W^B(x, y, \eta, t). \tag{30}$$

The case where there is a rigid wall at $z = 0$ can be treated by taking $\eta = 0$ and then simply setting

$$u_w = v_w = w_w = 0. \tag{31}$$

It is a straightforward matter to associate the boundary condition (27) on w with one of the governing equations; the prescribed wall-motion function w_w can be used to define a Dirichlet condition for the Poisson equation (9).

As noted in Section 1, the derivation of vorticity boundary conditions has been a source of difficulty for most previous velocity–vorticity methods. When transport equations for all three components of the vorticity are used in conjunction with all three Poisson equations (3), it would appear that a total of six boundary conditions must be imposed at the wall. The Poisson equations can be solved by using the boundary conditions on the velocity perturbations in a obvious manner, but the conditions required for the solution of the vorticity transport equations are not so readily supplied. Fasel and his collaborators [21, 23, 39, 54] made use of boundary conditions involving first and second derivatives of the perturbation velocity and vorticity components. This approach usually works well in practice but its limitations can be illustrated by considering an almost-parallel, two-dimensional, undisturbed flow along the x-direction. (This, of course, includes the case of Blasius flow over a flat plate studied by Fasel and his coworkers.) If attention is restricted to two-dimensional disturbances, there is only a single nonvanishing component of the perturbation vorticity, namely ω_y. Its evolution is governed by a transport equation of the form

$$\frac{\partial \omega_y}{\partial t} + U^B \frac{\partial \omega_y}{\partial x} + w \frac{\partial^2 U^B}{\partial z^2} + \text{non-parallel terms} + \text{nonlinear terms} = \frac{1}{R} \nabla^2 \omega_y. \tag{32}$$

It can be seen that, when nonparallel and nonlinear terms are neglected, there is no direct coupling between the perturbation vorticity ω_y and the streamwise perturbation velocity component u. For the transport equation (32) Fasel *et al.* used the vorticity boundary condition

$$\frac{\partial \omega_y}{\partial x} = -\frac{\partial^2 w}{\partial z^2} - \frac{\partial^2 w_w}{\partial x^2} \quad \text{for } z = \eta \tag{33}$$

obtained by substituting the boundary condition (27) for w into the Poisson equation (9). (Fasel *et al.* set $\eta = 0$ but allowed $w_w \neq 0$ in order to generate disturbances by suction and blowing at the wall.) It may be noted that no use has been made of the no-slip boundary condition. Thus, should an approximation of parallel undisturbed flow be applied and a linearization performed, the evolution of the vorticity would not be constrained, either directly or indirectly, by the no-slip condition on u. It follows that nonparallel or nonlinear terms must be retained in the vorticity transport equation (32) in order for there to be any prospect of obtaining a well-posed problem. Even then, the coupling between ω_y and u can be expected to remain weak if the effects of nonparallelism and nonlinearity are small. In fact, it can be formally argued that the scheme adopted by Fasel *et al.* remains ill-posed even if such effects are taken fully into account [13]. In practice, of course, this apparent difficulty has not prevented the nonparallel and nonlinear version of the scheme being used to conduct viable numerical simulations.

A major advantage of our formulation is that there is natural means of associating the wall-motion boundary conditions on u and v with the vorticity transport equations. We avoid the difficulties mentioned above by replacing wall boundary conditions for the vorticity with integral constraints obtained directly from the definitions (12) and (13) for the secondary variables with account taken of the conditions (25) and (26). Thus, we obtain

$$\int_\eta^\infty \omega_y \, dz = -u_w - \int_\eta^\infty \frac{\partial w}{\partial x} \, dz \tag{34}$$

$$\int_\eta^\infty \omega_x \, dz = v_w + \int_\eta^\infty \frac{\partial w}{\partial y} \, dz. \tag{35}$$

Since the substitution can be reversed, it is clear that these two relations are fully equivalent to the wall-motion boundary conditions for u and v. The relations (34) and (35) may thus be viewed as constraints on the evolution of the primary variables ω_y, ω_x, respectively. Each relation can be associated with one of the vorticity transport equations (7) and (8) to provide a means of satisfying the no-slip conditions, or their equivalents, for the fluid perturbation velocity. This ensures that the problem remains well-posed even when non-parallel and nonlinear terms are neglected or absent from the vorticity transport equations. Moreover, there is an attractive economy in the usage of the wall boundary conditions on the fluid perturbation velocities; each of the conditions for u, v, w is applied once, and once only, to provide conditions that constrain the development of ω_y, ω_x, and w, respectively.

2.3. *Wall-Normal Coordinate Mapping and the Conditions for $z \to \infty$*

As suggested earlier, there is no difficulty in implementing a condition on w in the limit $z \to \infty$. The vanishing of w provides a boundary condition for the solution of the Poisson equation (9). It is not so obvious how, in the same limit, the behavior of the other two primary variables, ω_x and ω_y, can be constrained. The secondary variables u and v are defined in such a way that they must both approach zero as $z \to \infty$. This implies that the limiting behavior of u and v cannot be used to obtain any additional constraint on ω_x and ω_y. Accordingly, such constraints must be obtained by some other means. In fact, we have already derived two further conditions that must be satisfied for $z \to \infty$, namely (19) and (23). Unfortunately, the first condition only constrains w, while the second one involves both components of the perturbation vorticity in a symmetric manner. As a consequence, there is no unambiguous way in which the two conditions can be associated with the individual transport equations for the vorticity components. In the present study, we will sidestep the issue by simply replacing the conditions (19) and (23) with the more easily implemented and stronger conditions that both ω_x and ω_y vanish for $z \to \infty$. We thus impose the same form of limiting behavior for all three of the primary variables. The validity of such an approach can be monitored, retrospectively, by checking that the primary variables computed using these replacement limiting conditions do, in fact, satisfy the conditions (19) and (23). Clearly, this consistency requirement would be met if it was found that the z-derivatives of all three of the computed primary variables vanished for $z \to \infty$. In practice, it is possible to obtain

satisfactory solutions by making use of the coordinate transformation

$$\zeta = \frac{l}{z+l}, \tag{36}$$

which maps the semi-infinite physical domain $z \in [0, \infty)$ on to the finite computational domain $\zeta \in (0, 1]$. The parameter l is a stretching factor. It can be seen that the limit $z \to \infty$ corresponds to the limit $\zeta \to 0$. Derivatives with respect to the physical coordinate z are related to those with respect to the transformed co-ordinate ζ according to

$$\frac{\partial f}{\partial z} = -\frac{\zeta^2}{l}\frac{\partial f}{\partial \zeta}, \tag{37}$$

so that it may be inferred that the z-derivative will vanish for $z \to \infty$ provided the ζ-derivative remains bounded as ζ approaches zero. Thus, if the primary variables are determined as functions of ζ, rather than z, it becomes a straightforward matter to determine whether the z-derivatives appearing in the conditions (19) and (23) vanish. We just need to check that the ζ-derivatives are bounded as $\zeta \to 0$. Consequently, provided our numerical simulations yield solutions for the primary variables which remain smooth functions of ζ when $\zeta \to 0$, the incompressibility condition and the transport equation for the wall-normal vorticity will automatically be satisfied. Further discussion concerning the usage of the mapping (36) is included in the section on numerical methods. In addition, a brief account is given in Appendix B of how the mapping could be modified to deal with a nonplanar flow boundary located at $z = \eta(x, y, t)$, for configurations where it is not appropriate to perform any linearization to obtain conditions to be applied at $z = 0$. For such cases, it is possible to perform a simple change of coordinates to obtain a modified set of governing equations for which the boundary conditions required at the physical boundary $z = \eta$ can be imposed along a planar computational boundary.

3. FORMULATION FOR THE ROTATING-DISC FLOW

3.1. *Transformation to Cylindrical Polar Coordinates*

Thus far, for expositional convenience, we have used a Cartesian coordinate system to present our velocity–vorticity formulation. However, it is not difficult to see that the formulation only relies upon a decomposition of the perturbation velocity and vorticity fields that combines projections in the z-direction with projections on to the orthogonal plane parallel to the wall. Hence, there is no problem changing to a cylindrical polar coordinate system; all that is involved is a transformation of coordinates in planes defined by constant values of z. It is also straightforward to change to a noninertial frame of reference rotating at a constant angular velocity about the z-axis. The only significant difference from the formulation for a nonrotating frame is that the Poisson equation (9) for w needs to be employed in order to recover the Coriolis term in the transport equation for ω_z. (There is no additional term to be included in the condition on the limiting behavior that corresponds to condition (23). The Coriolis term in the transport equation for ω_z is proportional to the derivative $\partial w/\partial z$, and so must vanish for $z \to \infty$ in accordance with (19), if the continuity equation is to be satisfied.)

For the rotating disc the velocity and vorticity fields may be represented as

$$\boldsymbol{u} = (u_r, u_\theta, w), \quad \boldsymbol{\omega} = (\omega_r, \omega_\theta, \omega_z),$$

where the subscripts r and θ refer, respectively, to the radial and azimuthal directions defined by the cylindrical polar coordinate system. The components $\{\omega_r, \omega_\theta, w\}$ can be taken as the primary variables, while $\{u_r, u_\theta, \omega_z\}$ form the set of secondary variables. The governing equations for the primary variables, obtained by transforming equations (7)–(9), take the form

$$\frac{\partial \omega_r}{\partial t} + \frac{1}{r}\frac{\partial N_z}{\partial \theta} - \frac{\partial N_\theta}{\partial z} - 2\Lambda\left(\omega_\theta + \frac{\partial w}{\partial r}\right) = \frac{1}{R}\left\{\left(\nabla^2 - \frac{1}{r^2}\right)\omega_r - \frac{2}{r^2}\frac{\partial \omega_\theta}{\partial \theta}\right\} \quad (38)$$

$$\frac{\partial \omega_\theta}{\partial t} + \frac{\partial N_r}{\partial z} - \frac{\partial N_z}{\partial r} + 2\Lambda\left(\omega_r - \frac{1}{r}\frac{\partial w}{\partial \theta}\right) = \frac{1}{R}\left\{\left(\nabla^2 - \frac{1}{r^2}\right)\omega_\theta + \frac{2}{r^2}\frac{\partial \omega_r}{\partial \theta}\right\} \quad (39)$$

$$\nabla^2 w = \frac{1}{r}\left(\frac{\partial \omega_r}{\partial \theta} - \frac{\partial (r\omega_\theta)}{\partial r}\right), \quad (40)$$

where $\boldsymbol{N} = (N_r, N_\theta, N_z)$ can be defined as previously by Eq. (10). There are additional terms on the left-hand sides of Eqs. (38) and (39) arising from the Coriolis acceleration. They have been written entirely in terms of the primary variables. The factor Λ represents the nondimensionalized angular velocity. In a similar manner to before, the secondary variables may be determined from the primary variables, using the explicit definitions

$$u_r = -\int_z^\infty \left(\omega_\theta + \frac{\partial w}{\partial r}\right) dz, \quad (41)$$

$$u_\theta = \int_z^\infty \left(\omega_r - \frac{1}{r}\frac{\partial w}{\partial \theta}\right) dz, \quad (42)$$

$$\omega_z = \frac{1}{r}\int_z^\infty \left(\frac{\partial (r\omega_r)}{\partial r} + \frac{\partial \omega_\theta}{\partial \theta}\right) dz. \quad (43)$$

3.2. *Undisturbed Flow*

The undisturbed flow is taken to be the laminar similarity solution of von Kármán [36] which is an exact solution to the Navier–Stokes equations for the flow field above a rotating disc in an unbounded fluid [55]. It is assumed that the disc rotates at a constant angular velocity Λ^* about the vertical z^*-axis, where asterisks denote dimensional quantities. The undisturbed base flow in a frame of reference rotating with the disc is given by

$$\boldsymbol{U}^{B*} = \left(U_r^{B*}, U_\theta^{B*}, W^{B*}\right). \quad (44)$$

These velocity components are related to the Kármán similarity variables as

$$F(z) = \frac{1}{r^*\Lambda^*}U_r^{B*}, \quad G(z) = \frac{1}{r^*\Lambda^*}U_\theta^{B*}, \quad H(z) = \frac{1}{(\nu^*\Lambda^*)^{\frac{1}{2}}}W^{B*}, \quad (45)$$

where ν^* is the kinematic viscosity and $z = z^*(\Lambda^*/\nu^*)^{1/2}$.

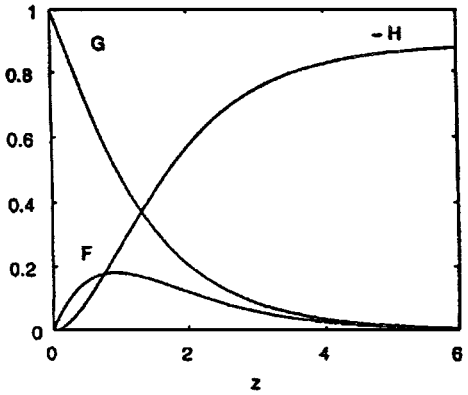

FIG. 2. Radial (F), azimuthal (G) and axial (H) velocity components for boundary layer flow over a rotating disc.

Thus, the nondimensional undisturbed flow is given by

$$\boldsymbol{U}^B = \left(\frac{r}{R}F, \frac{r}{R}G, \frac{1}{R}H\right), \tag{46}$$

where the Reynolds number R is defined as $R = r_a^*(\Lambda^*/\nu^*)^{1/2}$ for some selected radial position r_a^*. Since lengths are nondimensionalized using the fixed lengthscale $\delta^* = (\nu^*/\Lambda^*)^{1/2}$, we have $R = r_a$. It may also be noted that the nondimensionalized rotation rate is equal to $1/R$. Thus, when we choose to work in a frame of reference that rotates with the disc, it is necessary to set $\Lambda = 1/R$ for the Coriolis terms included in the vorticity transport equations (38) and (39). The velocity-profile functions F, G, and H are plotted in Fig. 2.

3.3. *Linearization and the Excitation of Azimuthal Modes*

In the present study we are interested in disturbances with vanishingly small amplitude, so we will use linearized governing equations. These are obtained by simply neglecting the nonlinear term $\boldsymbol{\omega} \times \boldsymbol{u}$ in the definition (10) of the quantity $\mathbf{N}$. The linearization makes the problem separable in the azimuthal direction which allows us to consider individual modes of the form

$$\boldsymbol{u} = (\hat{u}_r, \hat{u}_\theta, \hat{w})\, e^{in\theta}, \quad \boldsymbol{\omega} = (\hat{\omega}_r, \hat{\omega}_\theta, \hat{\omega}_z)\, e^{in\theta}, \tag{47}$$

where n is the integer-valued, azimuthal mode number. In order to excite disturbances in the boundary-layer flow, we will prescribe a radially localized motion of the disc surface with the same form of azimuthal variation. Because attention is restricted to small-amplitude disturbances, the boundary conditions may be linearized about the undisturbed wall, which is taken to be at $z = 0$. If it is supposed that the disc surface is only allowed to move in the vertical direction, the linearized boundary conditions may be written as

$$u_r = -\frac{r}{R}F'(0)\eta, \quad u_\theta = -\frac{r}{R}G'(0)\eta, \quad w = \frac{\partial \eta}{\partial t} \quad \text{at } z = 0, \tag{48a,b,c}$$

where $z = \eta(r, \theta, t)$ is the perturbed location of the disc surface. Substituting (48a) and (48b) into the definitions (41) and (42) of the secondary variables yields the following integral constraints on the primary variables

$$\int_0^\infty \omega_\theta \, dz = \frac{r}{R} F'(0)\eta - \int_0^\infty \frac{\partial w}{\partial r} \, dz \tag{49}$$

$$\int_0^\infty \omega_r \, dz = -\frac{r}{R} G'(0)\, \eta + \int_0^\infty \frac{inw}{r} \, dz, \tag{50}$$

where, as will frequently be the case in what follows, the assumed azimuthal mode structure has been used to replace partial derivatives with respect to θ by the multiplicative factor in.

In order to obtain a radially localized excitation of the fluid the wall displacement takes the form

$$\eta(r, \theta, t) = a(r - r_e)\, b(t)\, e^{in\theta}, \tag{51}$$

where the function a specifies the radial variation centred on the radius $r = r_e$ and the function b defines the time-dependent amplitude. Typically, we have employed radial distributions of the form

$$a(r) = e^{-\lambda r^2} e^{i\alpha r}, \tag{52}$$

where λ is a scaling factor which fixes the radial extent of the forcing and α is a wavenumber which, when not set equal to zero, may be chosen with the intention of enhancing the response for disturbances with a particular radial wavelength. The time-dependent amplitude may be chosen so as to give a time-periodic excitation, for instance by setting

$$b(t) = \left(1 - e^{-\sigma t^2}\right) e^{-i\beta t}, \tag{53}$$

where β is the prescribed temporal frequency and σ is a parameter chosen to scale the forcing up from zero amplitude at $t = 0$. Stationary disturbances, generated by stationary "bumps" on the disc surface distributed in accordance with the imposed azimuthal periodicity, can be considered by setting β equal to zero. Similarly, disturbances can be excited impulsively by employing

$$b(t) = \left(1 - e^{-\sigma t^2}\right) e^{-\sigma t^2} \tag{54}$$

or some other smoothed approximation to an impulse function.

As an alternative to exciting the flow by introducing a vertical wall motion, it is possible to specify a suction/blowing distribution. This can be achieved by dropping the terms involving η in the integral constraints (49) and (50) and replacing the condition on w by the requirement that $w = w_w$ at $z = 0$ where w_w is a prescribed function describing the character of the suction/blowing.

3.4. *Dynamics of the Compliant Wall*

The effects of wall compliance can be considered by embedding an annulus of compliant material within the otherwise rigid disc (see Fig. 3). The dynamics of the compliant wall may

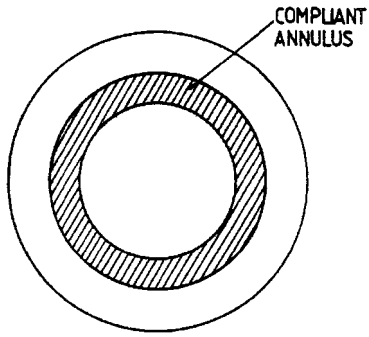

FIG. 3. Compliant annulus embedded within an otherwise rigid rotating disc.

be simulated using a spring-backed plate model, as in a previous study that was conducted for a different flow-configuration by Davies and Carpenter [14]. It is assumed that the compliant surface only moves in the z-direction. Denoting, as before, the wall displacement by $\eta(r, \theta, t)$, the equation of motion for the wall may be written as

$$m\,\frac{\partial^2\eta}{\partial t^2} + d\,\frac{\partial\eta}{\partial t} + B\,\hat{\nabla}^2\,\hat{\nabla}^2\eta + K\eta = -p_w, \tag{55}$$

where p_w is the fluid perturbation pressure acting at the wall, and $\hat{\nabla}^2$ is the two-dimensional Laplacian operator defined by

$$\hat{\nabla}^2 f = \frac{\partial^2 f}{\partial r^2} + \frac{1}{r}\frac{\partial f}{\partial r} + \frac{1}{r^2}\frac{\partial^2 f}{\partial\theta^2}.$$

The nondimensional parameters m, d, B, K are respectively the areal density, damping coefficient, flexural rigidity, and spring stiffness per unit area of the compliant wall. The perturbation pressure distribution can be found by integrating the linearized z-momentum component of the Navier–Stokes equations to obtain

$$p_w = \int_0^\infty \left\{ \frac{\partial w}{\partial t} + \frac{1}{R}\left(rF\frac{\partial w}{\partial r} + (G+1)\frac{\partial w}{\partial\theta}\right) + \frac{1}{rR}\left(\frac{\partial(r\omega_\theta)}{\partial r} - \frac{\partial\omega_r}{\partial\theta}\right)\right\} dz. \tag{56}$$

In practice, the terms involving the vorticity may be expected to be negligible at radial locations of interest. They will give contributions that are of the same order as the wall-normal viscous stresses that were ignored in Eq. (55). Assuming that some suitable means can be found for solving the equation of motion for the compliant wall, values for the displacement η and the wall velocity $\partial\eta/\partial t$ may be substituted into the linearized boundary conditions and vorticity integral constraints given in Eqs. (48)–(50). The only difference from before is one of interpretation. Near the forcing location $r = r_e$, the displacement η is simply prescribed, while within the compliant portion of the disc surface the displacement is interactively coupled to the fluid disturbances via the fluid perturbation pressure.

3.5. *Inflow and Outflow Conditions*

In many simulations of transitional boundary layers, the perturbation flow-fields are assumed to be periodic in two directions parallel to the wall [38]. This periodicity can

be built into the numerical methods, through the use of Fourier expansions, leading to highly efficient spectral codes. There is no guarantee that such an approach will lead to a satisfactory representation of spatially evolving disturbances, particularly when strong upstream influence is anticipated, or the wall boundary conditions are nonuniform. If the assumption of streamwise periodicity is dropped, it becomes necessary to address the issue of inflow and outflow conditions. The formulation of such conditions for the rotating-disc flow introduces some additional complications that are not encountered for two-dimensional boundary layers. If the computational domain is defined as $r_i \leq r \leq r_o$, where r_i and r_0 denote the radius of the inner and outer boundaries, respectively, then it is not at all obvious that it remains appropriate to use the terms "inflow" and "outflow" conditions. There is the distinct possibility that there will be significant propagation and growth of disturbances in the radially inward direction, as well as in the radially outward direction.

In practice, the inner radial boundary does not appear to cause any serious difficulties, provided that it is located at a sufficiently small radius. Disturbances can be expected to be increasingly damped as the disc centre is approached. Linear stability results [1, 43, 46] can be used as a guide. Assuming that a suitable selection of the inner radius r_i can be made, the simplest means of constraining the disturbance evolution at the boundary is to impose null values on an appropriate set of perturbation flow variables. For instance, all components of the perturbation velocity could be set to zero, giving the conditions that

$$u_r = u_\theta = w = 0 \quad \text{at } r = r_i. \tag{57}$$

Using the definitions (41) and (42) of the secondary variables, u_r and u_θ, these conditions can be translated into the following equivalent conditions on the primary variables:

$$\omega_\theta = -\frac{\partial w}{\partial r}, \quad \omega_r = w = 0 \ \text{ at } r = r_i. \tag{58}$$

Alternatively, the condition on ω_θ may be replaced by a straightforward null-value condition, giving the requirement that all of the primary variables vanish at the inner computational boundary, that is

$$\omega_\theta = \omega_r = w = 0 \quad \text{at } r = r_i. \tag{59}$$

In the numerical simulations, it was found that the results obtained using either conditions (58) or (59) were virtually identical, provided the inner radial boundary remained sufficiently removed from any source of disturbances.

The choice of boundary conditions at the outer radius of the computational domain must allow for the fact that in cases of interest, the boundary will lie in a region where disturbances are unstable. The difficulties this causes are exacerbated when there is strong radially inward influence and temporal disturbance growth. For our simulations, we considered three distinct strategies for dealing with the outer radial boundary. The simplest is to ensure that the outer radial boundary is always kept some distance away from locations where disturbances have evolved to appreciable amplitudes. Such an approach makes it unnecessary to model the behavior of disturbances at the outer boundary, but is computationally expensive.

The second strategy depends upon an assumption that the disturbances are wavelike at the outer radius, and involves the imposition of conditions of the form

$$\frac{\partial^2 \omega_r}{\partial r^2} = -\alpha^2 \omega_r, \quad \frac{\partial^2 \omega_\theta}{\partial r^2} = -\alpha^2 \omega_\theta, \quad \frac{\partial^2 w}{\partial r^2} = -\alpha^2 w \tag{60}$$

at $r = r_o$. The wavenumber α, which we can allow to be complex-valued to take account of spatial growth, can be set equal to the corresponding eigenvalue determined from linear stability theory. Since these boundary conditions can be imposed at a radial location where the disturbance amplitude is not negligible, the length of the computational domain may be significantly reduced. A similar approach has previously been applied, with some success, in studies of disturbance evolution in plane channel flow and Blasius flow (see for instance the works by Fasel [21], Fasel and Konzelmann [23] and Davies and Carpenter [14]). The validity of such wavelike boundary conditions usually depends upon the disturbance evolution remaining both linear and convective in nature. The first of these requirements is always met in the present numerical studies, since we only use linearized equations. The requirement that the disturbance convect through the outer radial boundary cannot, however, be so easily satisfied. When nonconvective behavior is anticipated, the simple wavelike boundary conditions (60) need to be applied with extreme caution if the disturbance is allowed to reach an appreciable amplitude at the outer radial computational boundary. (A more detailed discussion of the precautions that were necessary for rotating disc simulations involving absolute instability can be found in reference [16].) However, for the simulations that we have selected to report in detail in the present paper, the disturbance behavior remained purely convective. Under such circumstances, the wavelike conditions (60) were found to be perfectly adequate. Moreover, they proved to be particularly useful during code validation, when they facilated the use of relatively short computational domains.

The third strategy for dealing with the outer radial boundary is to add an outflow buffer region to the computational domain. A variety of different implementations of the buffer-region strategy have been applied in previous studies, for example as described by Bertolotti *et al.* [4], Kloker *et al.* [39] and Liu and Liu [45]. However, the success of such an approach, no matter how sophisticated in its implementation, can still be expected to depend upon whether or not the disturbances display a convective nature up to the beginning of the buffer region. Thus, in a sense, the buffer-region strategy involves little more than an elaboration of simple wavelike boundary conditions (60). It does, however, have the advantage that it can more readily cope with nonlinear disturbances and multimodal forms of disturbance whose behavior cannot be adequately modelled by simply prescribing a single outflow wavenumber. Nevertheless, the buffer region is only designed to allow disturbances to be convected out of the computational domain without spurious reflections. We do not claim to have undertaken extensive experimentation with the use of buffer regions for cases where nonconvective behaviour could be discerned, but our few tests suggest that, at least for linearized simulations involving only a single mode of disturbance, there was little advantage to be gained over the use of the simpler wavelike boundary conditions.

4. NUMERICAL METHODS

We will describe the numerical methods in the context of the rotating-disc problem, but the corresponding formulae for Cartesian coordinates should, for the most part, be fairly evident. We employ a mixed finite-difference/spectral method for the numerical discretization. The time-derivatives in the two vorticity transport equations (38) and (39) are discretized using a second-order scheme. For the sake of being definite, we will describe a particular three-point backward-difference scheme found to be robust for the most numerically challenging configuration that we have considered to date. Namely, the case where part of the disc

surface is compliant. For less demanding cases, where the disc's surface motion could be simply prescribed, a Crank–Nicholson/Adams–Bashforth type of time-stepping method was also implemented. This was more efficient than the method based on a three-point backward-difference scheme, when interactive calculations of the wall motion were not required. Further details are given in Appendix C.

Variations in the radial direction are discretized using a fourth-order, centered, compact finite-difference scheme. The wall-normal discretization is based upon a Chebyshev series representation using the mapped variable introduced in Eq. (36). We will focus our account of the numerical methods on features of the Chebyshev discretization that are of particular interest. It will be shown that is possible to obtain a discretization which is spectrally accurate in the z direction, but nevertheless involves only pentadiagonal operators acting on the Chebyshev expansion coefficients.

4.1. *Chebyshev Discretization for the Wall-Normal Variation*

Restricting attention to an individual azimuthal mode, the primary variables are expanded in terms of odd Chebyshev polynomials as follows

$$\omega_r(r,\theta,z,t) = \left\{ \sum_{k=1}^{M} \omega_{r_k}(r,t)\, T_{2k-1}(\zeta) \right\} e^{in\theta} \tag{61}$$

$$\omega_\theta(r,\theta,z,t) = \left\{ \sum_{k=1}^{M} \omega_{\theta_k}(r,t)\, T_{2k-1}(\zeta) \right\} e^{in\theta} \tag{62}$$

$$w(r,\theta,z,t) = \left\{ \sum_{k=1}^{M} w_k(r,t)\, T_{2k-1}(\zeta) \right\} e^{in\theta}, \tag{63}$$

where T_k is the kth Chebyshev polynomial and $\zeta \in (0,1]$ is the mapped wall-normal coordinate defined in Eq. (36). It is acceptable to use only the odd Chebyshev polynomials because our semi-infinite physical domain is mapped on to half of the usual Chebyshev interval. We assume, implicitly, that the primary variables and all of their even-order ζ-derivatives vanish for $\zeta \to 0$. This will certainly be the case if the disturbances decay exponentially for $z \to \infty$. (If for some flow variable f we have $f \sim e^{-sz}$ for $z \to \infty$, where $s > 0$, then we must also have $\partial^n f/\partial\zeta^n \to 0$ when $\zeta \to 0$ for all values of n.) The requirement that there is exponential decay of the disturbances should also be sufficient to ensure the coefficients in the Chebyshev expansion converge faster than any inverse power of their order [6].

The secondary variables may be expanded in terms of even Chebyshev polynomials

$$u_r(r,\theta,z,t) = \left\{ \frac{1}{2} u_{r_0}(r,t) + \sum_{k=1}^{M} u_{r_k}(r,t)\, T_{2k}(\zeta) \right\} e^{in\theta} \tag{64}$$

$$u_\theta(r,\theta,z,t) = \left\{ \frac{1}{2} u_{\theta_0}(r,t) + \sum_{k=1}^{M} u_{\theta_k}(r,t)\, T_{2k}(\zeta) \right\} e^{in\theta} \tag{65}$$

$$\omega_z(r,\theta,z,t) = \left\{ \frac{1}{2} \omega_{z_0}(r,t) + \sum_{k=1}^{M} \omega_{z_k}(r,t)\, T_{2k}(\zeta) \right\} e^{in\theta}, \tag{66}$$

where we set the zeroth-order expansion coefficient for u_r to be given by

$$u_{r_0}(r,t) = -2\sum_{k=1}^{M} u_{r_k}(r,t)\,(-1)^k, \tag{67}$$

and similarly for $u_{\theta_0}(r,t)$ and $\omega_{z_0}(r,t)$. This ensures that the secondary variables all vanish for $\zeta = 0$, i.e. for $z \to \infty$. Fixing the zeroth-order expansion coefficients in such a fashion is equivalent to expanding the secondary variables using a series of modified even Chebyshev polynomials $\bar{T}_{2k} = T_{2k} - T_{2k}(0)$.

The Chebyshev expansions for the primary and secondary variables can be substituted into the defining Eqs. (41)–(43) for the secondary variables to yield the following tridiagonal relations between the Chebyshev coefficients,

$$(k-1)u_{r_{k-1}} + 2ku_{r_k} + (k+1)u_{r_{k+1}} = -l\left(\omega_{\theta_k} - \omega_{\theta_{k+1}} + \frac{\partial}{\partial r}(w_k - w_{k+1})\right) \tag{68}$$

$$(k-1)u_{\theta_{k-1}} + 2ku_{\theta_k} + (k+1)u_{\theta_{k+1}} = l\left(\omega_{r_k} - \omega_{r_{k+1}} - \frac{in}{r}(w_k - w_{k+1})\right) \tag{69}$$

$$(k-1)\omega_{z_{k-1}} + 2k\omega_{z_k} + (k+1)\omega_{z_{k+1}} = \frac{l}{r}\left(\frac{\partial}{\partial r}\left(r\left(\omega_{r_k} - \omega_{r_{k+1}}\right)\right) + in\left(\omega_{\theta_k} - \omega_{\theta_{k+1}}\right)\right), \tag{70}$$

for $k = 1, \ldots, M$, where l is the stretching factor in Eq. (36) defining ζ. Details of the derivation are included in Appendix D. These relations can readily be used to determine the Chebyshev coefficients for the secondary variables from given values of those for the primary variables. All that is involved is a simple application of the Thomas algorithm. It should be remarked that the Chebyshev coefficients of the secondary variables are only required for the purposes of computing the convective terms in the vorticity transport equations. These involve the linearized quantity

$$\boldsymbol{N} = \boldsymbol{\Omega}^B \times \boldsymbol{u} + \boldsymbol{\omega} \times \boldsymbol{U}^B, \tag{71}$$

which is treated explicitly, via a predictor-corrector method, in the time-marching procedure. Thus, there is no need to allocate any permanent storage for the secondary variables; they only appear at an intermediate stage in the calculation of the quantity $\boldsymbol{N}$ from specified values of the primary variables. In fact, the representation of the secondary variables using Chebyshev coefficients can immediately be exchanged, via an application of a Fast Fourier Transform, for a representation in terms of collocation values. These collocation values can then be utilised in the pseudospectral evaluation of the mean-flow products in $\boldsymbol{N}$.

Before discussing the discretization of the governing equations we note that the integral conditions, (49) and (50), placed on the primary variables can be cast in the forms

$$\sum_{k=1}^{M} p_k \omega_{\theta_k} = \frac{r}{R} F'(0)\,\eta - \sum_{k=1}^{M} p_k \frac{\partial w_k}{\partial r} \tag{72}$$

$$\sum_{k=1}^{M} p_k \omega_{r_k} = -\frac{r}{R} G'(0)\,\eta + \sum_{k=1}^{M} p_k \frac{in w_k}{r} \tag{73}$$

for fixed constants p_k. These constraints on the primary-variable Chebyshev coefficients may be interpreted as discretized versions of the linearized no-slip conditions for the disturbances. The constants p_k can be computed by extending the argument used to derive the tridiagonal relations (68)–(70). More details are given in Appendix D. The boundary condition (48c) on w can be discretized in a more straightforward manner to yield

$$\sum_{k=1}^{M} q_k w_k = \frac{\partial \hat{\eta}}{\partial t}, \tag{74}$$

where $q_k = T_{2k-1}(1) = 1$ and the wall-displacement amplitude $\hat{\eta}$ is defined by writing $\eta(r, \theta, z, t) = \hat{\eta}(r, z, t)\, e^{in\theta}$.

The governing equations (38)–(40) are integrated twice with respect to the mapped variable ζ. This removes the z-derivative operators and replaces them with ζ-integral operators. Such a procedure is adopted because the integral operators take a very convenient form which facilitates the employment of an efficient line iteration along the radial direction. The integrated equations may be written as

$$\mathbf{I}\left[\frac{\partial \omega_r}{\partial t} + \frac{in}{r} N_z - 2\Lambda\left(\omega_\theta + \frac{\partial w}{\partial r}\right)\right] + \frac{1}{l}\,\mathbf{J} N_\theta \Bigg] = \frac{1}{R}\left\{\mathbf{I}\left[\left(\hat{\nabla}^2 - \frac{1}{r^2}\right)\omega_r - \frac{2in}{r^2}\omega_\theta\right] + \frac{1}{l^2}\,\mathbf{K}\,\omega_r\right\} \tag{75}$$

$$\mathbf{I}\left[\frac{\partial \omega_\theta}{\partial t} - \frac{\partial N_z}{\partial r} + 2\Lambda\left(\omega_r - \frac{in}{r} w\right)\right] - \frac{1}{l}\,\mathbf{J} N_r = \frac{1}{R}\left\{\mathbf{I}\left[\left(\hat{\nabla}^2 - \frac{1}{r^2}\right)\omega_\theta + \frac{2in}{r^2}\omega_r\right] + \frac{1}{l^2}\,\mathbf{K}\,\omega_\theta\right\} \tag{76}$$

$$\mathbf{I}\,\hat{\nabla}^2 w + \frac{1}{l^2}\,\mathbf{K} w = \mathbf{I}\left[\frac{in}{r}\omega_r - \frac{1}{r}\frac{\partial (r\omega_\theta)}{\partial r}\right], \tag{77}$$

where the integral operators **I**, **J**, and **K** are defined by

$$\mathbf{I} f(\zeta) = \int^{\zeta}\int^{\zeta'} f(\zeta'')\, d\zeta'\, d\zeta''$$

$$\mathbf{J} f(\zeta) = \int^{\zeta} \zeta'^2 f(\zeta')\, d\zeta' - 2\int^{\zeta}\int^{\zeta'} \zeta'' f(\zeta'')\, d\zeta'\, d\zeta''$$

$$\mathbf{K} f(\zeta) = \zeta^4 f(\zeta) - 6\int^{\zeta} \zeta'^3 f(\zeta')\, d\zeta' + 6\int^{\zeta}\int^{\zeta'} \zeta''^2 f(\zeta'')\, d\zeta'\, d\zeta'',$$

and, using the assumed form of the azimuthal variation,

$$\hat{\nabla}^2 f = \frac{\partial^2 f}{\partial r^2} + \frac{1}{r}\frac{\partial f}{\partial r} - \frac{n^2}{r^2} f$$

for any function f. When they are applied to an appropriate Chebyshev series, the integral operators can be represented by banded matrices that are, at most, pentadiagonal, except for the lowest-order terms. For instance, the integral operator **I** acts on series of odd Chebyshev

polynomials in the following tridiagonal manner

$$\mathbf{I}\sum_{k=1}^{M} f_k\, T_{2k-1} = a\, T_0 + b\, T_1 + \sum_{k=2}^{M+1} \frac{1}{8}\left(\frac{f_{k-1}}{(2k-1)(k-1)} - \frac{f_k}{(k-1)k} + \frac{f_{k+1}}{(2k-1)k}\right) T_{2k-1}, \quad (78)$$

where the arbitrary integration constants a, b arise from the double indefinite integration. A similar, but pentadiagonal, representation can be obtained for the operator **K**. The integral operator **J**, which acts on the series of even Chebyshev polynomials used to approximate the quantities N_θ and N_r, can be represented by a matrix with a bandwidth of four.

Substituting the Chebyshev series for the primary variables into the integrated governing equations and then matching the coefficients of T_{2k-1} for $k = 2, \ldots, M$ leads to a system of $3(M-1)$ partial differential equations for the $3M$ unknowns $\{\omega_{r_k}, \omega_{\theta_k}, w_k\}$. The three equations that would have been obtained by matching the coefficients of the lowest-order odd polynomial T_1 can be dispensed with because they only serve to introduce additional unknowns in the form of integration functions. They are replaced by the conditions given in Eqs. (72)–(74) corresponding to the wall boundary conditions for the fluid disturbance velocity components, the no-slip conditions having first been formulated as the equivalent integral constraints on the vorticity. We then obtain a set of $3M$ partial differential equations for the $3M$ unknown Chebyshev coefficients of the primary variables. This procedure may be classified as a form of the tau-method.

4.2. *Temporal and Radial Discretization*

Using the notation

$$f^l = f|_{t=l\Delta t}$$

the three-point, backward-difference, time discretization takes the form

$$\left(\frac{\partial f}{\partial t}\right)^l = \frac{1}{2\Delta t}(3f^l - 4f^{l-1} + f^{l-2}). \quad (79)$$

The time-stepping is performed using a predictor-corrector scheme for the convective terms in the integrated vorticity transport equations. The Coriolis terms in the transport equations may be dealt with either implicitly or by applying the same predictor-corrector that is used for the convective terms. The predictor-corrector method can also be chosen for some selected viscous terms arising from the use of a non-Cartesian coordinate system. The remaining viscous terms, which involve double indefinite ζ-integrals of second-order derivatives along each of the r, θ, z coordinate directions, can all be treated implicitly. The Poisson equation for w and all of the boundary conditions, including the integral constraints on the vorticity, are also applied in an implicit manner. (In what follows we will assume, for the sake of being definite, that the Coriolis terms and selected viscous terms are computed using a predictor-corrector. The modifications required for an implicit treatment of all but the convective terms would introduce only marginal differences in the computational cost.)

The predictor step for the convective terms, which requires the evaluation of the quantity $\boldsymbol{N}$, is specified by setting

$$\begin{aligned}(\boldsymbol{N}^l)^p &= 2\,\boldsymbol{N}^{l-1} - \boldsymbol{N}^{l-2} \\ &= 2(\boldsymbol{\Omega}^B \times \boldsymbol{u}^{l-1} + \boldsymbol{\omega}^{l-1} \times \boldsymbol{U}^B) - (\boldsymbol{\Omega}^B \times \boldsymbol{u}^{l-2} + \boldsymbol{\omega}^{l-2} \times \boldsymbol{U}^B),\end{aligned} \tag{80}$$

while the corrector step is defined by

$$(\boldsymbol{N}^l)^c = \boldsymbol{N}((\boldsymbol{u}^l)^p, (\boldsymbol{\omega}^l)^p) = \boldsymbol{\Omega}^B \times (\boldsymbol{u}^l)^p + (\boldsymbol{\omega}^l)^p \times \boldsymbol{U}^B, \tag{81}$$

where $(\boldsymbol{u}^l)^p$, $(\boldsymbol{\omega}^l)^p$ are the disturbance velocity and vorticity fields determined from the predictor stage. This time stepping process involves two evaluations of the undisturbed-flow product terms per time step. In addition, because of the implicit treatment of some of the remaining terms in the governing equations, there is a large system of linear equations that must be solved twice per time step. As mentioned previously, the products involving undisturbed-flow quantities are calculated in a pseudospectral manner using a Fast Fourier Transform to convert between Chebyshev series coefficients and collocation values and *vice versa*. When the predictor-corrector employed for the convective terms is also applied to the Coriolis terms and appropriately selected viscous terms, the relevant Chebyshev series coefficients can be evaluated directly without resort to any transformation.

The Crank–Nicholson method, used in conjunction with an Adams–Bashforth treatment of the convective terms, might appear at first sight to be a more obvious, less computationally expensive, choice for the time-stepping procedure. However, on the basis of our previous experience [14] we expected a backward-difference method to perform more robustly, particularly when there is interactive wall-motion. The advantages of such time-stepping procedures have also been documented in other circumstances where there is motion at a fluid boundary (see, for example, [5]). Nevertheless, we make no claim that the particular time-stepping procedure that we have elected to describe here in detail has been optimized. For simulations that did not involve any interactively coupled wall motion, improvements to the efficiency of the numerical scheme were readily made by treating more terms in an explicit manner and adopting a modified predictor-corrector method. (As was mentioned earlier, further details of the alternative time-stepping procedure can be found in Appendix C.)

Introducing the notation

$$f^l_{k,j} = f_k|_{r=j\Delta r, t=l\Delta t},$$

where, as before, the suffix k is used to denote a Chebyshev series coefficient, the discretization of the governing equations can be completed by approximating the radial derivatives using compact, fourth-order, centered, finite-difference schemes of the general form:

$$\begin{aligned}&\alpha\left(\frac{\partial f^l}{\partial r}\right)_{k,j-1} + \left(\frac{\partial f^l}{\partial r}\right)_{k,j} + \alpha\left(\frac{\partial f^l}{\partial r}\right)_{k,j+1} \\ &\quad = \frac{2(\alpha+2)}{3}\left(\frac{f^l_{k,j+1} - f^l_{k,j-1}}{2\Delta r}\right) + \frac{4\alpha-1}{3}\left(\frac{f^l_{k,j+2} - f^l_{k,j-2}}{4\Delta r}\right),\end{aligned} \tag{82}$$

$$\beta\left(\frac{\partial^2 f^l}{\partial r^2}\right)_{k,j-1}+\left(\frac{\partial^2 f^l}{\partial r^2}\right)_{k,j}+\beta\left(\frac{\partial^2 f^l}{\partial r^2}\right)_{k,j+1}$$
$$=\frac{4(1-\beta)}{3}\left(\frac{f^l_{k,j+1}-2f^l_{k,j}+f^l_{k,j-1}}{(\Delta r)^2}\right)+\frac{10\beta-1}{3}\left(\frac{f^l_{k,j+2}-2f^l_{k,j}+f^l_{k,j-2}}{4(\Delta r)^2}\right). \tag{83}$$

In principle, the parameters α, β can be freely chosen. The choices $\alpha = 1/4$, $\beta = 1/10$ minimize the stencil of discrete radial locations involved in the computation of the first and second derivatives. Most of our computations were performed using these values. Setting $\alpha = \beta$ allows both first- and second-order radial derivatives to be completely eliminated from the fully discretized governing equations, which is more convenient when computer storage is at a premium. We conducted a few simulations with $\alpha = \beta = 1/10$ and obtained results that were virtually identical to those obtained with $\alpha = 1/4$, $\beta = 1/10$.

The finite-difference approximations for the radial derivatives may be employed together with the temporal discretization to obtain discretized versions of the partial differential equations for the primary-variable Chebyshev coefficients discussed in Section 4.1. The full set of $3M$ partial differential equations contains three subsets of M equations that are associated, in turn, with the two vorticity transport equations and the Poisson equation for w. The first equation in each M-equation subset is chosen to be the condition that enforces the appropriate boundary condition on the fluid perturbation velocity at the wall, while the remaining $M-1$ equations are obtained directly from the integrated governing equation. Using the notation

$$\boldsymbol{F}^l_j = \left(f^l_{1,j},\, f^l_{2,j}, \ldots,\, f^l_{M,j}\right)^T,$$

for vectors of Chebyshev coefficients, the fully discretized governing equations can be written in the forms

$$\boldsymbol{S}_j\boldsymbol{\Omega}^l_{\boldsymbol{r}j} = \boldsymbol{B}^l_{\boldsymbol{r}j} + \boldsymbol{C}^l_{\boldsymbol{r}j}, \quad \boldsymbol{S}_j\boldsymbol{\Omega}^l_{\boldsymbol{\theta}j} = \boldsymbol{B}^l_{\boldsymbol{\theta}j} + \boldsymbol{C}^l_{\boldsymbol{\theta}j}, \quad \boldsymbol{T}_j\boldsymbol{W}^l_j = \boldsymbol{B}^l_{wj}, \tag{84}$$

where $\{\boldsymbol{\Omega}^l_{\boldsymbol{r}j}, \boldsymbol{\Omega}^l_{\boldsymbol{\theta}j}, \boldsymbol{W}^l_j\}$ represent the Chebyshev vectors of the primary variables $\{\omega_r, \omega_\theta, w\}$ and $\boldsymbol{S}_j$, $\boldsymbol{T}_j$ are $M \times M$ matrices. The vector $\boldsymbol{B}^l_{\boldsymbol{r}j}$ is a simple linear function of vectors $\boldsymbol{\Omega}^l_{\boldsymbol{r}i}$ for $i \neq j$ and the vector $\boldsymbol{W}^l_j$, the latter being involved because the integral constraint coupling ω_r and w is incorporated as the first component of the vector equation. The vectors $\boldsymbol{B}^l_{\boldsymbol{\theta}j}$, $\boldsymbol{B}^l_{\boldsymbol{w}j}$ are specified in a similar manner; the former can be computed using vectors other than $\boldsymbol{\Omega}^l_{\boldsymbol{\theta}j}$ and the latter computed from vectors other than $\boldsymbol{W}^l_j$. In the two fully discretized vorticity transport equations, the vectors $\boldsymbol{C}^l_{\boldsymbol{r}j}$ and $\boldsymbol{C}^l_{\boldsymbol{\theta}j}$ collect together quantities which can be calculated explicitly using the primary-variable vector values from the previous two time steps and, in the corrector stage of the time stepping, from the primary-variable vectors computed during the predictor stage. There is no corresponding vector in the fully discretized Poisson equation for w because the equation is treated in a fully implicit fashion.

The matrices $\boldsymbol{S}_j$, $\boldsymbol{T}_j$ are pentadiagonal except for their first rows. This pentadiagonal structure is the consequence of our choosing to replace z-derivative operators by ζ-integral operators for the purposes of the Chebyshev discretization. The first rows of the matrices are used to incorporate the perturbation velocity boundary conditions at the wall. It should be recalled that the conditions to be imposed on the primary variables $\{\omega_r, \omega_\theta, w\}$ were stated in Eqs. (72)–(74). Because the coefficients p_k, q_k appearing in these condition are nonzero for $k = 1, \ldots M$, the first rows of the matrice $\boldsymbol{S}_j$, $\boldsymbol{T}_j$ are full.

It may be seen that the fully-discretized equations (84), have been cast in a form that is well-suited for efficient solution by means of a line iteration along the radial direction. The inversions required to obtain estimates for each of the primary-variable Chebyshev vectors $\{\boldsymbol{\Omega}_{\boldsymbol{r}j}^l, \boldsymbol{\Omega}_{\boldsymbol{\theta}j}^l, \boldsymbol{W}_j^l\}$ at a given radial location, using previous estimates for the vectors at locations that are radially inward and outward from the given location, can be performed by employing a pentadiagonal equation solver that is modified to take account of the full first rows of the matrices $\boldsymbol{S}_j$, $\boldsymbol{T}_j$.

4.3. *Numerical Solution for the Compliant-Wall Motion*

When an annular region of the wall is compliant (see Fig. 3), values of the wall displacement must be supplied to specify the boundary conditions for the fluid motion. In order to obtain a stable numerical scheme, the equation of motion (55) for the wall must be recast in form

$$\frac{\partial}{\partial t}\left(m w_s + \int_0^\infty w\, dz\right) + d\, w_s + B\, \hat{\nabla}^2\, \hat{\nabla}^2 \eta + K\eta$$
$$= -\frac{1}{R}\int_0^\infty \left\{ rF\frac{\partial w}{\partial r} + (G+1)\frac{\partial w}{\partial \theta} + \frac{1}{r}\left(\frac{\partial (r\omega_\theta)}{\partial r} - \frac{\partial \omega_r}{\partial \theta}\right)\right\} dz, \tag{85}$$

where boundary condition (48c) has been used and we have substituted the expression (56) for the fluid perturbation pressure at the wall. Equation (85) can be viewed as an evolution equation for the total wall-normal momentum defined by

$$\mu = m w_s + \int_0^\infty w\, dz. \tag{86}$$

The compliant-wall and hydrodynamic momenta are combined in order to avoid the domination of one over the other when they are included in the radial line iteration outlined in Section 4.2. When this is not done, the iteration can fail to converge. The details of how the reformulated equation of motion for the compliant wall may be employed to derive a numerically stable coupling between the wall and the fluid are similar to those that were presented in [14], to which the interested reader should refer. For present purposes it suffices to note two important features. First, the fully-discretized boundary condition for w may be implemented in the modified form

$$\sum_{k=1}^{M} (\gamma_j\, p_k + q_k)\, w_{k,j}^l = \tilde{w}_j^l, \tag{87}$$

where γ_j is defined in terms of the wall parameters and the discretization constants. (The coefficients p_k, q_k which are used, respectively, to evaluate w at the wall and its integral across the boundary layer, were defined in Section 4.1.) The variable $\tilde{w}_j^l$ appearing on the right-hand side of (87) can be calculated using vectors other than $\boldsymbol{W}_j^l$. Thus, it may determined within the radial line-iteration procedure. Secondly, we note that the fully discretized version of the unmodified boundary condition on w, which was stated in a partially discretized form in Eq. (74), may be written as

$$\hat{\eta}_j^l = \frac{1}{3}\left(4\,\hat{\eta}_j^{l-1} - \hat{\eta}_j^{l-2}\right) + \frac{2\Delta t}{3}\sum_{k=1}^{M} q_k w_{j,k}^l \tag{88}$$

where

$$\hat{\eta}_j^l = \hat{\eta}|_{r=j\Delta r, t=l\Delta t}.$$

This can be used to determine the wall displacement amplitude $\hat{\eta}$, that must be known in order to impose the integral constraints on the vorticity, when the boundary condition applied directly to w is cast in the form (87).

5. SIMULATION RESULTS FOR CONVECTIVE DISTURBANCES IN THE ROTATING-DISC BOUNDARY LAYER

5.1. *Stationary Disturbances and Code Validation*

We undertook extensive validation of our computer code through simulations of the disturbances in the rotating-disc boundary layer. Initially, the governing equations were "parallelized" (i.e., slow radial change was neglected) so that direct comparisons could be made with results from previous linear-stability studies [12, 46–48]. The "parallelization" was achieved by neglecting the radial dependence of the coefficients which multiply the differential operators appearing in the governing equations (38)–(40) and the definitions (41)–(43) of the secondary variables. All the coefficients were set to constant values by simply substituting the fixed Reynolds number R for the variable radius r.

Radial wavenumbers and growth rates determined from the "parallelized" numerical simulations were compared with corresponding eigenvalues determined from the linear stability theory of previous investigators. (The specific form of the sixth-order system of ordinary differential equations, and the numerical method used for their solution, are described in reference [12]). Good agreement was found over a range of Reynolds numbers for a variety of stationary and time-periodic forms of disturbance, including both Type I and Type II instabilities.

Comparisons were also made for numerical simulations based on the complete linearized Navier–Stokes equations. It was found that locally defined radial wavenumbers and growth rates computed from the numerical simulations could be well-predicted using the eigenvalues obtained from standard, (i.e., quasi-parallel), linear stability theory. This is illustrated in Fig. 4, which shows radial wavenumbers and growth rates for the case of a stationary disturbance with azimuthal mode number $n = 32$. (This is the most strongly growing eigenmode.) In the numerical simulations, the disturbance was excited by introducing bumps on the wall in the manner described in Section 3.3. The maximum wall displacement was located at $r = 350$. Locally defined, complex, radial wavenumbers $\alpha = \alpha_r + i\alpha_i$ could be computed using the simulation data by setting

$$\alpha^2 = -\frac{1}{A}\frac{\partial^2 A}{\partial r^2}, \tag{89}$$

where A is the complex amplitude of some selected flow-field variable. For the results presented in Fig. 4, the complex radial wavenumber was calculated using the amplitude of the integral of ω_θ across the boundary layer. It can be seen that, away from radial locations close to where the wall deformation is greatest, the radial wavenumbers and growth rates agree well with standard linear stability theory. The oscillations in the curves near $r = 350$ are a reflection of near-field effects in the simulations; the disturbance only has a well-defined complex radial wavenumber at a sufficient radial distance from its source.

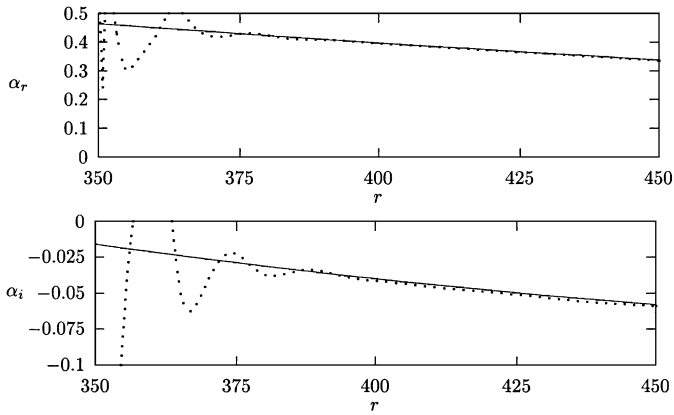

FIG. 4. Radial wavenumbers α_r and radial growth rates α_i for a stationary disturbance with azimuthal wavenumber $n = 32$. The solid curves were determind by solving, for each of the Reynolds number over the range of radii, the eigenvalue problem derived by applying the parallel-flow approximation. The dotted curves correspond to locally calculated complex radial wavenumbers obtained directly from numerical simulation data.

The numerical-resolution requirements for the simulations were established by undertaking extensive and detailed, grid-refinement studies. It was found that, typically, the variation of the primary perturbation variables ω_r, ω_θ, w across the boundary layer in the z-direction, could be fully resolved using a Chebyshev expansion involving 48 polynomials. The radial resolution was selected to give at least 24 points per wavelength, which usually translated to taking a radial increment $\Delta r \simeq 1$. The temporal resolution was dictated by the convergence demands of the line-iteration scheme used to solve the set of implicit equations obtained at each time step, rather than by accuracy requirements. Typically, the need to obtain a converged solution led to a choice of time increment $\Delta t \simeq \Delta r$ that was sufficient for full resolution of the temporal evolution when the Reynolds number R was $O(10^3)$ or less. (It should be noted that, with the specified nondimensionalization, the Reynolds number is equal to the value of the dimensionless radial coordinate at the inner radius of the computational domain.) The nondimensional rotation period T for the disc is equal to $2\pi R$. Thus, it may be seen that our typical choice of time-increment was such that $\Delta t/T \sim 10^{-3}$. In addition, as has mentioned above, the effects of the positions of the inner and outer computational radial boundaries were carefully monitored. For most of the simulations, the computational domain extended well beyond the limits suggested by the figures used to illustrate the behavior of physical interest. For example, the perturbation velocity fields for the time-periodic Type I disturbances considered at beginning of the next section are displayed for $375 \leq r \leq 525$, whereas the simulations were actually conducted using a computational domain with $250 \leq r \leq 950$.

5.2. *Nonstationary Type I and II Disturbances*

In order to further illustrate the utility of our numerical simulation method, we provide a brief description of results for the radial evolution of Type I and Type II travelling-wave disturbances. Both types of disturbance were excited by prescribing a radially localized, time-periodic, wall displacement, with a nondimensional frequency βR. The form of the wall motion used for the excitation was described in Section 3.3.

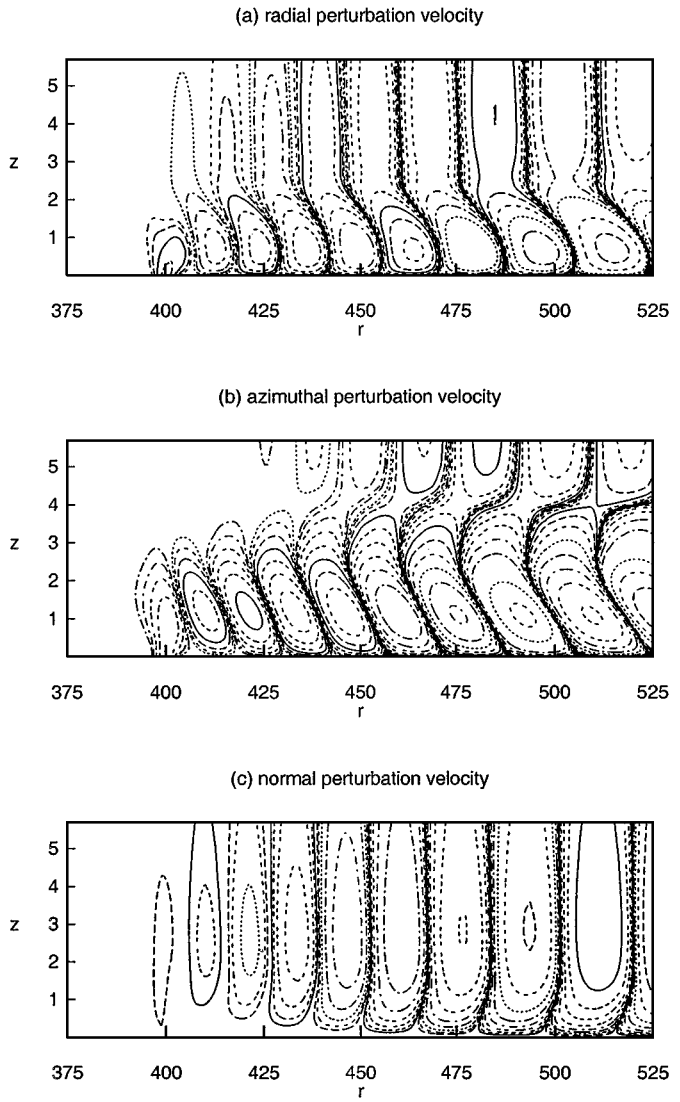

FIG. 5. Perturbation velocity contours for a Type I disturbance with $n = 43$ and $\beta R = -8$, excited by localized disk surface motion centred at $r_e = 400$. The contours are drawn at levels $\pm A2^m$ for $m = 0, 1 \ldots, N$, where A is an arbitary normalization factor and N defines the contour level corresponding to the largest disturbance magnitudes. The normalization remains the same for each of the plotted perturbation velocity components but the value of N varies: (a) u_r; $N = 11$, (b) u_θ; $N = 12$, (c) w; $N = 8$. Thus, the z-component of the perturbation velocity can be seen to be an order of magnitude smaller than the other two components.

Figure 5 displays perturbation velocity contours, at a particular instant of time and a fixed value of the azimuthal angle, for a Type I disturbance with azimuthal mode number $n = 43$. The disturbance was excited by setting the nondimensional wall-motion frequency $\beta R = -8$. The forcing was centred on $r_e = 400$. Both the n and βR were chosen so that, according to standard linear stability theory, the radial growth rate would be as large as possible at radial locations close to excitation. The pronounced radial growth experienced by the disturbance can be inferred from the contour plots upon noting the logarithmic scale

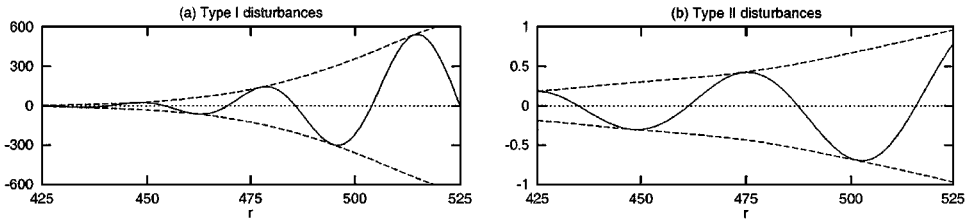

FIG. 6. Perturbation azimuthal vorticity ω_θ at the disk surface (solid lines), together with corresponding envelopes $\pm|\omega_\theta|$ (broken lines), for Type I and Type II disturbances exicted at $r_e = 400$. (a) $n = 43$ and $\beta R = -8$ (b) $n = 5$ and $\beta R = 7.9$ The amplitudes are normalized so that, in both cases, ω_θ is $O(1)$ at locations near to where the disturbances are generated.

used to define the contour levels. This radial growth can also be discerned, more readily, from Fig. 6a, which displays the radial variation of ω_θ at the disc surface. The time instant and the azimuthal orientation are the same as for Fig. 5. Figure 6b shows the corresponding result for the Type II disturbance, which, according to the standard linear stability theory, should undergo maximal radial growth at the chosen radial location $r_e = 400$. In this case, $n = 5$ and $\beta R = 7.9$. It can be seen that, as expected from previous studies, the radial growth of the Type II disturbance is much weaker than that exhibited by the Type I disturbance. In particular, it should be noted that the amplitude of the localized wall motion, used as excitation, has been normalized in a commensurable fashion for both types of disturbance. Thus, the large differences between the magnitudes of the perturbation vorticities, at radial locations away from the source of excitation, reflect the disparity between the radial growth rates of the two disturbance types. The difference in the radial growth rate is also apparent from the contour plots given in Fig. 7. By making a comparison with Fig. 5, it can be seen that the two types of disturbance also differ in other respects. For instance, there is a marked contrast between the radial wavelengths. There are also differences in the distance above the disc surface where the perturbation velocities achieve their maxima.

5.3. *The Effects of Wall Compliance*

The different characters of the Type I and Type II disturbances remained evident when simulations were conducted for configurations where a compliant annulus was inserted in the rotating-disc surface, as shown in Fig. 3. Figure 8 illustrates the stabilizing effect on Type I disturbances of having such a compliant insert between $r = 450$ and 500. The figure shows the instantaneous radial variation of the wall pressure, at a fixed azimuthal angle for a case where the disc surface was taken to be entirely rigid, compared with a corresponding case where there was a compliant insert. The wall displacement is also plotted. As before, the disturbance was excited by time-periodic wall motion centered on $r = 400$. It is clear that wall compliance leads to a significant reduction in the disturbance growth in the radial direction, even though the compliant annulus extends for less than two disturbance wavelengths. This is in accordance with the results of the standard linear stability of Cooper and Carpenter [12] for compliant walls in the form of a single layer of elastomeric material, the dynamics of which were modelled using modified Navier equations.

The wall parameters m, B, K defining our simpler spring-backed-plate model were selected so that no flow-induced surface instabilities would be expected over the range of radii considered. (It should be recalled from Section 3.4 that m, B, K are, respectively, the

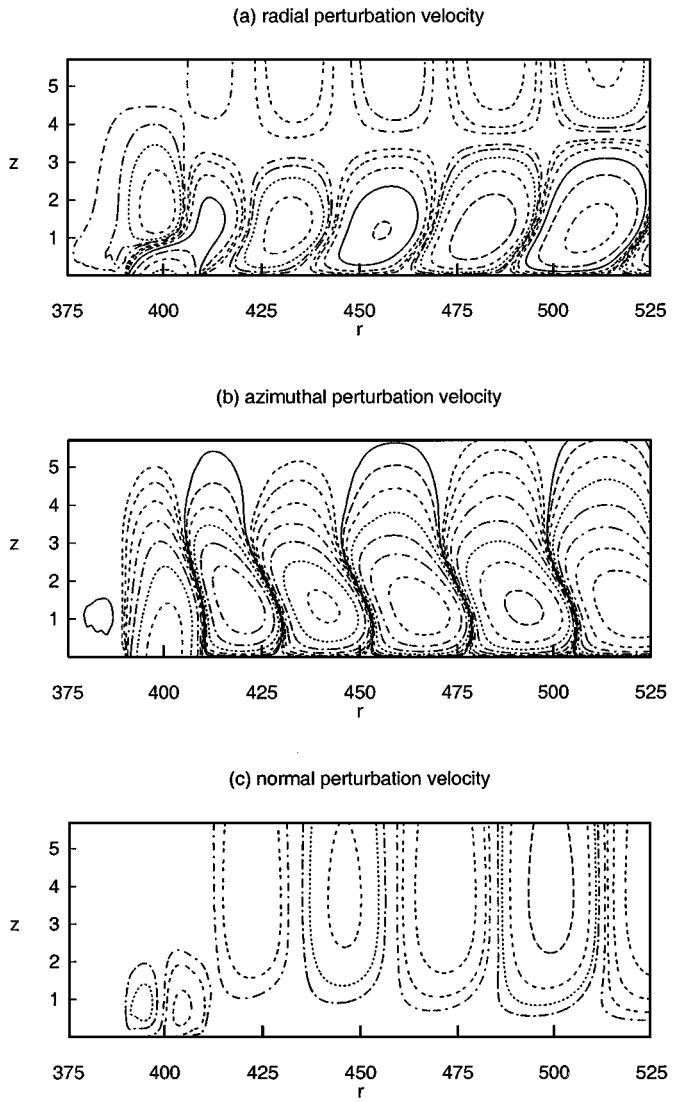

FIG. 7. Perurbation velocity contours for a Type II disturbance with $n = 5$ and $\beta R = 7.9$, exited by localised disk surface motion centered at $r_e = 400$. The contours are drawn at levels $\pm A2^m$ for $m = 0, 1 \ldots, N$, in the same manner as in Fig. 5. (a) u_r; $N = 6$, (b) u_θ; $N = 7$, (c) w; $N = 5$.

nondimensional areal density, flexural rigidity, and spring stiffness for the compliant wall.) Crude estimates for the onset velocities of flow-induced surface instabilities were derived by modelling the undisturbed von Kármán flow as a uniform rotational flow and then assuming that established results for the case of uniform uni-directional flow over a compliant plate [10] could be applied in a localized manner. Such a procedure leads to two restrictions on the choice of the nondimensional wall parameters, each of which gives a recipe for the avoidance of a distinct mode of flow-induced surface instability. These restrictions can then be applied to choose the wall parameters to make the compliant annulus as soft as possible without introducing any flow-induced surface instability. When such a choice is made, the wall parameters m, B, K can all be specified in terms of a single critical wavenumber

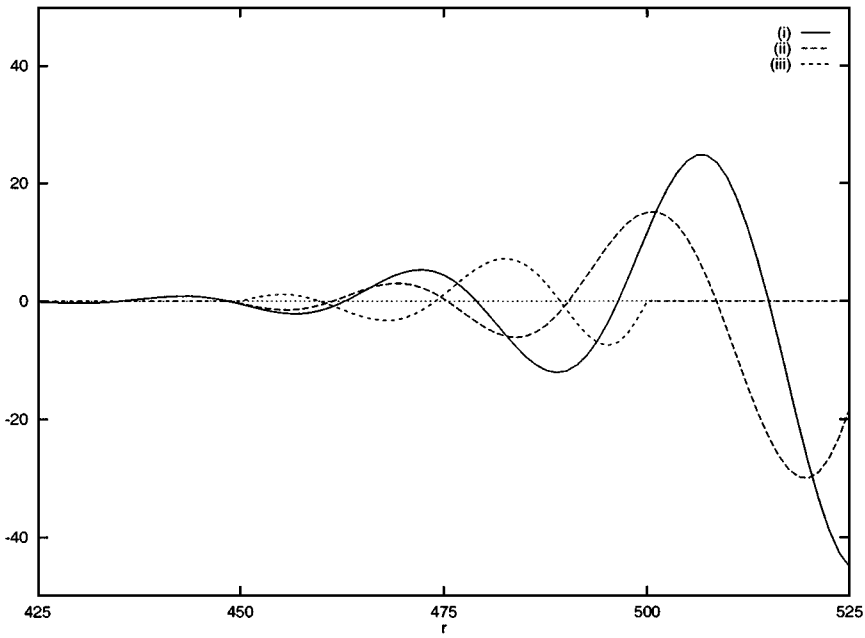

FIG. 8. Instantaneous surface displacements and perturbation pressures at the disk surface for a Type I disturbance with $n = 43$ and $\beta R = -8$ exicted at $r = 400$. (i) Pressure for an entirely rigid disk, (ii) pressure at the same time instant in the periodic forcing cycle when there is a compliant annulus which extends from $r = 450$ to $r = 500$, (iii) corresponding compliant surface displacements. The surface compliance parameters are such that, notionally, there is marginal stability with respect to divergence and travelling wave flutter forms of disturbance at the outermost radius of the annulus. The critical wavenumber for the compliant surface is $\alpha_c = 0.2$.

defined by

$$\alpha_c = \left(\frac{K}{3B}\right)^{\frac{1}{4}} . \tag{90}$$

The compliant part of the disc surface would only be expected to give rise to significant stabilizing effects on Type I disturbances when α_c is selected so as to be comparable with the wavenumbers of the most unstable Type I disturbances. Accordingly, we set $\alpha_c = 0.2$ for the simulation presented here. (For a more detailed discussion of these matters, in the context of plane channel flow between compliant walls, the interested reader should refer to [15].)

Simulations were also conducted to investigate the effect of wall compliance on Type II disturbances. The changes identified in the radial growth rates were negligible when the wall parameters were selected in the above manner. This null result concurs with the work of Cooper and Carpenter [12], who found that the modification of Type II disturbances resulting from wall compliance was rather weak, compared with Type I disturbances.

5.4. *Algebraic Radial Growth*

Modal coalescence between Type I and Type II disturbances has been studied, independently, by Lingwood [43], Cooper and Carpenter [12], and Turkyilmazoglu and Gajjar [58].

The standard linear stability analysis carried out by these previous investigators predicted that modal coalescence would first occur at $R = 437$ for a temporal frequency $\beta = 0.0061$ and an azimuthal wavenumber given by $n/R = 0.041$ (which, it should be noted, actually corresponds to an unphysical noninteger value of $n = 17.9$). They found that the coalesced eigenmode was convectively stable at its onset Reynolds number. Examination of the solution branches for the spatio-temporal eigenvalue problem also established that the modal coalescence did not give rise to an absolute instability. There remained the interesting possibility that the coalesced eigenmode could exhibit prolonged algebraic growth [40]. However, upon closer scrutiny, the physical significance of any such algebraic growth might appear to be rather limited. Quasi-parallel linear stability theory predicts that, at above a Reynolds number $R \simeq 439$, which is only very slightly higher than the Reynolds number of $R = 437$ corresponding to the onset of modal coalescence, the coalesced mode becomes convectively unstable. Thus, when the slow radial variation is properly accounted for, it is likely that any algebraic radial growth would be eclipsed by exponential radial growth over a relatively short radial distance. Notwithstanding this, there is still some purpose to be achieved from a brief study of disturbance development when modal coalescence is expected. Numerical simulations can be used to examine the effects of "nonparallelism" and to verify that algebraic radial growth does, in fact, occur within the framework of the "parallel-flow" approximation. Moreover, the successful identification of algebraic radial growth in simulations conducted with "parallelized" governing equations can be viewed as providing an additional stringent validation for the computer code.

Figure 9 displays "parallelized" numerical simulation results for the radial variation of ω_θ at the wall for the case of a time-periodic disturbance at the predicted onset of modal coalescence $R = 437$. A cursory inspection suggests that the disturbance is subject to algebraic growth, rather than the exponential decay expected in the absence of modal coalescence. Stronger confirmation of the predictions of the quasi-parallel linear stability theory of Cooper and Carpenter can be inferred from the excellent fit to the simulation data

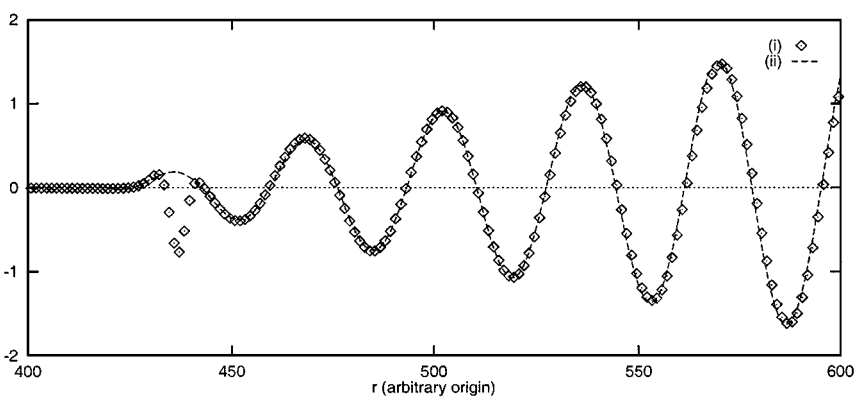

FIG. 9. Instantaneous azimuthal vorticity ω_θ at the surface of a rigid disk for the modal coalescence involving the Type I and Type II forms of disturbance. $R = 437$, $n/R = 0.041$ and $\beta = 0.0061$. (i) Numerical simulation results obtained with the parallel-flow approximation applied to the fluid governing equations, (ii) data-fit using a function $\Omega(r) = (r - r_e)\,\Re\{Ae^{i\alpha(r-r_e)}\}$, where r_e locates the time-periodic forcing, A is a fixed complex constant and $\alpha = 0.185 + 0.0015i$ is the complex radial wavenumber. (Note that, owing to use of the parallel-flow approximation, the origin of the radial co-ordinate system is arbitrary.)

that is shown for a function of the form

$$\Omega(r) = (r - r_e)\,\Re\left\{A\,e^{i\alpha(r-r_e)}\right\} \quad \text{for } r \geq r_e, \tag{91}$$

where r_e defines the innermost radial location at which there is time-periodic forcing. The term A is a complex constant that fixes the arbitrary phase and amplitude and α is the complex radial wavenumber. The value $\alpha = 0.185 + 0.0015\,i$ selected for the wavenumber was determined, independently of the results of the numerical simulation, using the quasi-parallel linear stability theory for the specified azimuthal wavenumber $n/R = 0.041$ and temporal frequency $\beta = 0.0061$. It can be seen from Fig. 9 that deviations between the fitted function and the simulation data are only found in the immediate vicinity of the locations where time-periodic wall motion is used to generate the disturbance. They can thus be discounted as being attributable to near-field effects. It should be noted that the disturbance would have slowly decayed, over a radial lengthscale $1/\alpha_i \sim 10^3$ if algebraic growth were absent.

The effects on the modal coalescence of using the complete linearized Navier–Stokes equations are illustrated in Fig. 10. Radial distributions of the ω_θ amplitudes are plotted for numerical simulations conducted with and without the use of the "parallel flow" approximation. The time-periodic forcing used to excite the disturbance was applied in the same manner with the same normalization, in both cases. An amplitude distribution fitted using the eigenvalue α determined from the standard linear stability theory is also displayed. In order to facilitate comparisons, a slight geometric inconsistency is accommodated for the "nonparallel" case. The azimuthal mode number n is permitted to be noninteger valued, just as before. (Similar results were obtained from other simulations for which n was, more correctly, taken to be an integer.) Inspection of the plotted simulation data suggests that there is still a region of algebraic radial growth when the complete linearized Navier–Stokes equations are used. However, in so far as it can be identified with any precision, the region of algebraic growth does not appear to extend very far beyond the source of the disturbance. It can also be seen that, close to the source of the disturbance, the radial growth appears to be slightly weaker than for standard linear theory. As expected, the algebraic growth gives way to exponential radial growth, when convective instability sets in further outboard.

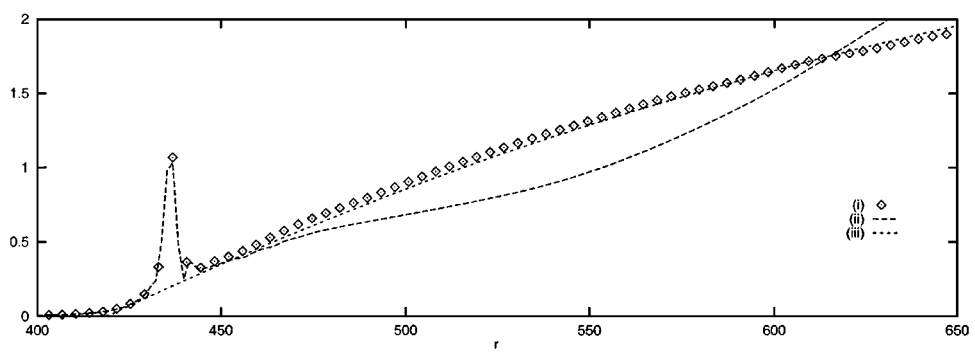

FIG. 10. Azimuthal vorticity amplitude $|\omega_\theta|$ at the surface of a rigid disk for the modal coalescence involving the Type I and Type II forms of disturbance. $R = 437$, $n/R = 0.041$ and $\beta = 0.0061$. Simulation results obtained with (i) the parallel-flow approximation, (ii) nonparallel mean flow effects included. (iii) Data-fit using a function $|\Omega(r)| = (r - r_e)|A|e^{-\alpha_i(r-r_e)}$, where $\alpha_i = 0.0015$ is the imaginary part of the complex radial wavenumber obtained from the solution of the parallel-flow linear stability eigenvalue problem, r_e locates the time-periodic forcing and A is a fixed constant.

6. CONCLUSIONS

We have described a new velocity–vorticity formulation of the unsteady three-dimensional Navier–Stokes equations. The approach is designed to be suitable for simulating the evolution of three-dimensional disturbances in boundary-layer flows, particularly for flow-control applications. It is assumed that the undisturbed flow field is known. (As shown in Appendix A, this is not an essential assumption.) Accordingly, only perturbations to this known flow field are calculated. In general, the perturbations are of finite amplitude. A key advantage of the formulation is that only *three* governing equations for three primary dependent variables are required. The three primary variables are the perturbations to the wall-normal velocity component and to the two vorticity components in the plane of the wall. The secondary variables are the perturbations to the remaining velocity and vorticity components and, for some applications, the pressure. These are defined explicitly in terms of the primary variables. We show that, providing the primary variables can be made to satisfy certain fairly weak conditions as $z \to \infty$, our formulation is fully equivalent to the Navier–Stokes equations in primitive-variable form.

For our formulation, only three dependent variables need to be computed and stored. This contrasts favourably to previous three-dimensional, velocity–vorticity formulations (e.g., Fasel and his coworkers) which require all six velocity and vorticity components to be primary variables. Our approach even offers advantage compared with the primitive-variable formulation with its four dependent variables. Thus, since our formulation only employs three flow-field variables and three governing equations, it offers considerable scope for improvements in algorithm design and computational times in applications involving direct numerical simulations of boundary-layer disturbances. Another important advantage offered by our approach lies in the treatment of the constraints placed on vorticity. The apparent need for vorticity boundary conditions has been problematic with previous velocity–vorticity methods. We show that the wall boundary conditions placed on velocity may be linked to vorticity through integral constraints. Such an approach ensures solenoidal velocity and vorticity fields and provides a simple and rigorous alternative to vorticity boundary conditions.

The numerical methods were presented in the context of application to the three-dimensional boundary layer over a rotating disc. However, the corresponding methodology for a Cartesian coordinate system should, for the most part, be fairly evident. Our scheme of discretization employs spectral expansions in the wall-normal and azithmuthal (or spanwise) directions and compact finite differences in the radial (or streamwise) direction. Discretization in time takes the form of a three-point, backward-difference scheme. Time stepping is based on a predictor-corrector scheme for the convective terms. For the application to the rotating disc, but not for those using Cartesian coordinates, the predictor-corrector scheme is also used for the Coriolis and some viscous terms. The remaining viscous terms (all viscous terms in applications based on Cartesian coordinates) can be treated implicitly. It is shown that we can retain an efficient line-iteration scheme, similar to that used by Fasel [21] and in his later papers, but with the added advantage of spectral convergence in the wall-normal direction. (For simulations that do not involve any interactive wall motion, the line-iteration scheme can be simplified. The radial line iteration used to determine the vorticity may be replaced by a more direct, radial line-marching procedure as described in Appendix C.)

For some of the applications reported above we have used a compliant wall. Wall compliance is, of course, a passive method of flow control. Nevertheless, computationally it is

much more challenging than active boundary-layer control methods such as suction and blowing or the use of MEMS- or micro-actuators. In such cases, the wall boundary conditions are normally specified *a priori*. Whereas for a compliant wall, the calculation of wall and flow dynamics must be carried out interactively. In such circumstances, it can be difficult to achieve a stable numerical scheme. In our previous work [14] on the simulation of the development of two-dimensional boundary-layer disturbances over compliant walls, we overcame the problem of achieving a stable scheme by combining the flow and wall momenta as, effectively, a single variable. In the present paper, we show how this approach can be extended to the three-dimensional case.

The applications presented in the present paper concern convective disturbances developing in the boundary layer over a rotating disc. (Investigations of absolute instabilities in the same system will be reported in a separate paper. A preliminary account is given in reference [16].) The simulations are restricted to small-amplitude disturbances for which the governing equations can be linearized. This permits us to decouple the azimuthal modes and compute them separately, thereby making the simulations much less computationally expensive. It also allows us to validate the methods by comparison with known results from standard linear stability analysis. We excite the most unstable stationary Type I instability by introducing small-amplitude bumps on the disc surface. Good agreement is found with previous linear-stability results. In our standard formulation, we use the full linearized governing equations without suppressing the slow radial variation of the disturbances. In fact, we find that the results are not greatly different from the standard, "parallel-flow," linear stability theory which omits the slow radial variation. This is in accord with the PSE results of Malik and Balakumar [47]. We have also studied the travelling forms of the Type I and Type II instabilities over rigid and compliant walls. Finally, we simulated the case where the standard, linear, stability theory predicts a coalescence between Types I and II eigenmodes. Theory suggests that, even though the disturbances are convectively stable, coalescence implies localized algebraic growth. This is confirmed by the "parallelized" simulations. When the full linearized governing equations were used, localized algebraic growth was still observed, but exponentially growing convective instability set in at slightly more outboard locations and soon dominated the algebraic growth.

The present application for the rotating disc has been restricted to small-amplitude disturbances and only linearized governing equations were used. It is not too difficult to see how the scheme could be generalized to allow the simulation of nonlinear finite-amplitude disturbances. In this case, the nonlinear terms introduce coupling between the various azimuthal modes and we would be unable to compute them separately. However, if, like the convective terms in the linearized case, the nonlinear terms were treated explicitly within the time-marching procedure, essentially the same line-iteration process could be used for the nonlinear computations. The main difference would be the need to repeat the radial line-iteration solution procedure for every resolved azimuthal mode, possibly using some form of parallel processing. The nonlinear terms would only generate quantities which remained fixed within the radial line iteration undertaken for each time step, in much the same manner as was described for the convective terms in the linearized case.

We end by briefly mentioning some of the further applications of the new velocity–vorticity formulation that have been made to date. This serves to emphasize the fact that the utility of the formulation is by no means restricted to the rotating disc flow that we considered in detail in the present paper. For example, the linearized version of the governing equations has been used to simulate interactions between MEMS actuators and various forms of

small-amplitude three-dimensional disturbances developing in the Blasius boundary layer and other laminar boundary layers. These simulations were conducted using essentially the same numerical scheme as described in the present paper. The only significant change, aside from the incorporation of MEMS devices and some new methods of disturbance generation, was that a Cartesian coordinate system was used, instead of the cylindrical polar coordinates that were more appropriate for the rotating disc. Careful code validation was undertaken, in the same manner as for the simulations reported in the present paper. In particular, we found that it was possible to reproduce standard linear stability results for both two- and three-dimensional disturbances developing within the boundary layer. We were also able to undertake more demanding simulations that involved the development of disturbances that extended out beyond the boundary layer and into the free-stream. More details can be found in reference [11].

In addition to studies conducted for three-dimensional linear disturbances, we have undertaken some simulations of two-dimensional, fully nonlinear, disturbance development in Blasius flow [34]. (A short account of the two-dimensional restriction of the velocity–vorticity formulation is given in Appendix E.) The disturbance evolution was investigated both with and without the use of the parallel flow approximation. Good agreement was found with the behavior predicted by large Reynolds number asymptotic theories. Moreover, the numerical simulation code remained robust even when the Reynolds number, based on displacement thickness, was taken to be in excess of 10^5.

A two-dimensional version of our velocity–vorticity formulation has also been used to compute the steady wake flow near the trailing edge of an aligned flat plate. For this inherently nonlinear computation, the vorticity integral constraint used to impose no-slip along the surface of the plate was replaced by a center-line symmetry condition within the wake itself. The computed steady flow was found to develop, along the streamwise direction, in precisely the manner predicted by triple-deck asymptotic theory (see, for example, [35]).

APPENDIX A

Velocity–Vorticity Formulation for the Total Flow and for Finite Domains

For the present study of the rotating-disc boundary layer, the undisturbed flow can be determined directly from the solution of a set of ordinary differential equations [55]. Thus, there would be little interest in using our formulation to determine the undisturbed flow. This may not be the case for other potential applications. We will now describe how our formulation may be modified to deal with the undisturbed flow or, more generally, with the total flow. If we set $\mathbf{U}^B = \mathbf{\Omega}^B = 0$ in the decomposition defined in Eqs. (6a) and (6b) then the total velocity and vorticity field $\mathbf{U}$, $\mathbf{\Omega}$ are identical with the fields previously taken to be perturbations, and the definition of the convective quantity $\mathbf{N}$ becomes

$$\mathbf{N} = \mathbf{\Omega} \times \mathbf{U}.$$

If, in order to conform with the notation used in the main text, we take the components of $\mathbf{U} = (u, v, w)$ and $\mathbf{\Omega} = (\omega_x, \omega_y, \omega_z)$, the three governing equations (7)–(9) can now be interpreted as equations for the total-flow primary variables. It remains to specify the total-flow secondary variables $\{u, v, \omega_z\}$ in terms of the primary variables. Allowing for the fact

that **U** may no longer vanish for $z \to \infty$, we set

$$u = -\int_z^\infty \left(\omega_y + \frac{\partial w}{\partial x}\right) dz + \bar{u}_\infty$$

$$v = \int_z^\infty \left(\omega_x - \frac{\partial w}{\partial y}\right) dz + \bar{v}_\infty$$

$$\omega_z = \int_z^\infty \left(\frac{\partial \omega_x}{\partial x} + \frac{\partial \omega_y}{\partial y}\right) dz + \bar{\omega}_{z_\infty},$$

where $\bar{u}_\infty$, $\bar{v}_\infty$ are the prescribed velocity components for $z \to \infty$ and

$$\bar{\omega}_{z_\infty} = \frac{\partial \bar{v}_\infty}{\partial x} - \frac{\partial \bar{u}_\infty}{\partial y}.$$

For example, for a zero-pressure gradient flow over a flat plate we would simply have

$$\bar{u}_\infty = 1, \quad \bar{v}_\infty = \bar{\omega}_{z_\infty} = 0.$$

The argument used to recover the primitive-variables form of the Navier–Stokes equations for the perturbation flow fields can be reapplied to the case of the total flow fields. The only difference is that the conditions which must be imposed on the primary variables for $z \to \infty$, in order to recover the incompressibility constraint and the z-component of the vorticity transport equation, both take a slightly more complicated form. For instance, it is necessary to ensure that

$$\frac{\partial w}{\partial z} \to -\left(\frac{\partial \bar{u}_\infty}{\partial x} + \frac{\partial \bar{v}_\infty}{\partial y}\right) \quad \text{for } z \to \infty$$

in order to obtain the incompressibility constraint.

It is of interest to note that the formulation could, in principle, be extended to cases where there is an upper boundary at $z = L$. This would involve replacing the $z \to \infty$ upper limit by $z = L$ in the integrals defining the secondary variables. It would also be necessary to impose the incompressibility constraint and the z-component of the vorticity transport equation at the location $z = L$. For example, if there were a rigid stationary boundary located at $z = L$ (where L is constant), then the definitions of secondary variables would be given by

$$u = -\int_z^L \left(\omega_y + \frac{\partial w}{\partial x}\right) dz,$$

$$v = \int_z^L \left(\omega_x - \frac{\partial w}{\partial y}\right) dz,$$

$$\omega_z = \int_z^L \left(\frac{\partial \omega_x}{\partial x} + \frac{\partial \omega_y}{\partial y}\right) dz,$$

while the conditions to be imposed at $z = L$ would take the simple form

$$\frac{\partial w}{\partial z} = \frac{1}{R}\frac{\partial}{\partial z}\left(\frac{\partial \omega_x}{\partial x} + \frac{\partial \omega_y}{\partial y}\right) = 0.$$

APPENDIX B

Coordinate Mapping for the Case of a Nonplanar Boundary

The system of equations that comprises the new velocity–vorticity formulation is first described in the main part of the text for a general configuration where there is a bounding surface located at $z = \eta(x, y, t)$. However, for the specific application that is considered in detail, namely the evolution of small-amplitude disturbances in the rotating disk boundary layer, a linearization is performed, giving boundary conditions that are applied at $z = 0$. In this section we provide a brief account of how the velocity–vorticity formulation, including the boundary conditions, can be implemented in a computationally convenient fashion when the flow boundary is taken to be more genuinely nonplanar and when it is not appropriate to apply any form of linearization.

We suppose, as before, that the flow occupies the semi-infinite region region $\eta \leq z < \infty$ and introduce the simple change of coordinates $Z = z - \eta(x, y, t)$, which maps the boundary at $z = \eta(x, y, t)$ on to the plane defined by $Z = 0$. (More generally we could also incorporate a transformation of the form $X = f(x, y, t)$, $Y = g(x, y, t)$ in the x-y plane. Such a transformation was used, implicitly, when cylindrical polar coordinates were applied in a rotating frame for our study of the rotating disk boundary layer flow. However, we omit any further details here in the interests of brevity.) By making the substitutions

$$\tilde{\omega}_x(x, y, Z, t) = \omega_x(x, y, z, t),$$
$$\tilde{\omega}_y(x, y, Z, t) = \omega_y(x, y, z, t),$$
$$\tilde{w}(x, y, Z, t) = w(x, y, z, t),$$

for the primary variables $\{\omega_x, \omega_y, w\}$, and similarly for the secondary variables $\{u, v, \omega_z\}$, the two vorticity transport equations, the Poisson equation and the secondary variable definitions can all be transformed in a straightforward manner to yield a system in which both the primary variables and the secondary variables, as well as the differential and integral operators that act upon them, are expressed in terms of Z, rather than z. Of particular interest are the transformed definitions of the secondary variables. These take the form

$$\tilde{u} = -\int_Z^\infty \left(\tilde{\omega}_y + \frac{\partial \tilde{w}}{\partial x}\right) dZ - \frac{\partial \eta}{\partial x}\,\tilde{w},$$
$$\tilde{v} = \int_Z^\infty \left(\tilde{\omega}_x - \frac{\partial \tilde{w}}{\partial y}\right) dZ - \frac{\partial \eta}{\partial y}\,\tilde{w},$$
$$\tilde{\omega}_z = \int_Z^\infty \left(\frac{\partial \tilde{\omega}_x}{\partial x} + \frac{\partial \tilde{\omega}_y}{\partial y}\right) dZ + \frac{\partial \eta}{\partial x}\,\tilde{\omega}_x + \frac{\partial \eta}{\partial y}\,\tilde{\omega}_y.$$

As would be expected, the secondary variables are still defined explicitly in terms of the primary variables. The only change is that there are some additional terms that involve the slope of the nonplanar physical boundary. Using the above definitions of the secondary variables, it may be readily shown that the no-slip conditions stated in Section 2.2 can be

cast as vorticity integral conditions that take the form

$$\int_0^\infty \tilde{\omega}_y \, dZ = -u_w - \int_0^\infty \frac{\partial \tilde{w}}{\partial x} \, dZ - \frac{\partial \eta}{\partial x} w_w,$$

$$\int_0^\infty \tilde{\omega}_x \, dZ = v_w + \int_0^\infty \frac{\partial \tilde{w}}{\partial y} \, dZ + \frac{\partial \eta}{\partial y} w_w,$$

where u_w, v_w, w_w are the prescribed velocities for $z = \eta$, as in Eqs. (25)–(27). Thus, the no-slip conditions can be imposed using constraints that only involve integration over the fixed semi-infinite interval $0 \leq Z < \infty$. Finally, we note that the wall-normal coordinate mapping considered in Section 2.3 can be applied to Z, rather than z, to map the semi-infinite domain $Z \in [0, \infty)$ on to a finite computational domain. Thus, we set

$$\zeta = \frac{l}{Z + l},$$

where l is a mapping constant, to obtain a computational domain such that $\zeta \in (0, 1]$. A discretization based upon Chebyshev expansions can then be applied for the wall-normal variation, as described in Section 4.

APPENDIX C

An Alternative Time-Stepping Method

In Section 4.2 we described a time-stepping method that employs a second-order, three-point, backward-difference formula for the time derivatives. This formula was applied in conjunction with a predictor-corrector method for the convective terms in the vorticity transport equations. The decision to implement the time integration in such a fashion was motivated by our previous experience in simulating fluid-structure interactions for a two-dimensional flow [14]. We had found that the use of a fully implicit time-stepping procedure could provide a robust means of overcoming numerical stability problems. However, in the absence of any interactive coupling between the motion of the fluid and its bounding walls, the conditions required for numerical stability can be relaxed. This allows more explicit time-stepping methods to be adopted.

Accordingly, for cases without any interactive wall motion coupling, we have developed and implemented a Crank–Nicholson/Adams–Bashforth type of method for the time stepping. In this alternative numerical scheme, all the terms appearing in the vorticity transport equations, with the exception of those viscous terms involving z-derivatives, can be treated in an explicit fashion by means of a predictor-corrector scheme. It is also possible to treat the vorticity integral constraints in an explicit manner. The advantage of the resulting discretization scheme is that the two primary-variable vorticity components can be determined directly, at every radial location, prior to the solution of the Poisson equation for w. The modified scheme for obtaining the each vorticity component thus involves only a single radial line march, rather than the more expensive radial line iteration described previously. Line iteration is still needed to solve the Poisson equation, but w can now be constructed using already determined values of the vorticity.

The improvements to the time-stepping procedure can be illustrated by re-employing the notation that was first introduced in Section 4.2. In the same manner as for Eq. (84), the

discretized equations to be solved at each time step may be cast in the form,

$$\mathbf{S}\boldsymbol{\Omega}_{r\,j}^{l} = \mathbf{C}_{r\,j}^{l},$$
$$\mathbf{S}\boldsymbol{\Omega}_{\theta\,j}^{l} = \mathbf{C}_{\theta\,j}^{l},$$
$$\mathbf{T}_j\mathbf{W}_j^{l} = \mathbf{B}_{w\,j}^{l} + \mathbf{D}_{w\,j}^{l},$$

where the matrix $\mathbf{S}$ is now independent of the radial location. The right-hand sides of the two discretized vorticity transport equations can be computed explicitly, using known values of the primary variables. Thus, the terms $\mathbf{B}_{r\,j}^{l}$ and $\mathbf{B}_{\theta\,j}^{l}$ appearing in Eq. (84) are no longer present. Because the matrix $\mathbf{S}$ remains pentadiagonal, apart from its first row, the Chebyshev vectors $\boldsymbol{\Omega}_{r\,j}^{l}$ and $\boldsymbol{\Omega}_{\theta\,j}^{l}$ can be determined from $\mathbf{C}_{r\,j}^{l}$ and $\mathbf{C}_{\theta\,j}^{l}$ in a very efficient manner. The right-hand side of the discretized Poisson equation contains an additional term $\mathbf{D}_{w\,j}^{l}$, denoting the quantities that can be computed directly, without any need for iteration, from the previously determined values of $\boldsymbol{\Omega}_{r\,j}^{l}$ and $\boldsymbol{\Omega}_{\theta\,j}^{l}$. The vector $\mathbf{B}_{w\,j}^{l}$ is now defined so that it depends only on the values of w at locations that are radially inward or outward from the selected radial position. Plainly, then, radial line iteration is still required in order to obtain the Chebyshev vectors $\mathbf{W}_j^{l}$.

To summarize, it may be stated that in the alternative time-stepping scheme, radial line iteration is replaced by a single radial line march for each of the vorticity transport equations; but a slightly modified, radial line iteration is retained for the Poisson equation. In the main body of the text there are a number of references to radial line iterations. When interactive wall motion is not involved, most of these references should, strictly speaking, be replaced by a reference to the radial line marching/radial line iteration combination outlined immediately above.

APPENDIX D

Chebyshev Discretization for the Secondary Variables

The definitions of the secondary variables take the general form

$$f = \int_z^{\infty} g\, dz,$$

where f is the secondary variable and g is specified in terms of the primary variables and their derivatives in the planes orthogonal to the z-direction. Introducing the coordinate mapping $\zeta = l/(z+l)$, which maps the semi-infinite interval $[0, \infty)$ to the finite interval $(0, \zeta]$, yields the relationship

$$f = l\int_0^{\zeta} \frac{g}{\zeta^2}\, d\zeta.$$

Setting

$$g = \sum_{k=1}^{\infty} g_k\, T_{2k-1}(\zeta), \quad h = \frac{g}{\zeta^2} = \sum_{k=1}^{\infty} h_k T_{2k-1}(\zeta),$$

and using the fact that

$$\zeta^2 T_{2k-1} = \frac{1}{4}(T_{2k+1} + 2T_{2k-1} + T_{2k-3}),$$

we can conclude that

$$g_k = \frac{1}{4}(h_{k-1} + 2h_k + h_{k+1}).$$

We also have

$$\int_0^\zeta h\, d\zeta = \frac{1}{4}\sum_{k=1}^{\infty} \frac{1}{k}(h_k - h_{k+1})(T_{2k}(\zeta) - T_{2k}(0)),$$

where we have employed the identity

$$4T_{2k-1} = \frac{1}{k}T'_{2k} - \frac{1}{k-1}T'_{2(k-1)}$$

for $k > 1$. Thus, we can set

$$f = \sum_{k=1}^{\infty} f_k \left(T_{2k}(\zeta) - T_{2k}(0)\right),$$

where

$$f_k = \frac{l}{4k}(h_k - h_{k+1}).$$

Hence, as may easily be checked,

$$(k+1)\, f_{k+1} + 2k f_k + (k-1)\, f_{k-1} = \frac{l}{4}(h_{k-1} + 2h_k + h_{k+1} - (h_k + 2h_{k+1} + h_{k+2})).$$

Using the relation between the Chebyshev coefficients of g and h given earlier, we can remove all reference to the intermediate variable h. We thus obtain

$$(k+1)\, f_{k+1} + 2k f_k + (k-1)\, f_{k-1} = l(g_k - g_{k+1}),$$

which, when truncated to finite order, is the relationship that was used to derive the tridiagonal schemes for the secondary-variable Chebyshev coefficients given in Eqs. (68)–(70).

Finally, we outline the method used to compute the constants p_k which are required for the numerical evaluation of integrals across the boundary layer. Such integrals appear in the integral constraints imposed on the vorticity and also in the expression for the perturbation fluid pressure at the solid surface. For the case of untruncated Chebyshev expansions, the constants p_k may be defined by setting

$$f|_{z=0} = \int_0^\infty g\, dz = \sum_{k=1}^{\infty} p_k g_k.$$

For the finite-order truncation, the constants may be determined by first computing the matrix P_{jk} which satisfies

$$(k-1)P_{j,k-1} + 2kP_{j,k} + (k+1)P_{j,k+1} = \delta_{j,k} - \delta_{j,k+1}$$

for $j, k = 1, \ldots, M$, and then setting

$$p_k = 2l \sum_{j=1}^{M/2} P_{k,2j-1},$$

as may be demonstrated by applying the previously obtained relationship between the Chebyshev coefficients f_k, g_k to evaluate $f|_{z=0} = f|_{\zeta=1}$ when $g_k = \delta_{j,k}$.

APPENDIX E

Two-Dimensional Version of the Velocity–Vorticity Formulation

With a view to the applications mentioned in the concluding section of the main part of the paper, we present the two-dimensional restriction of the velocity–vorticity formulation for the case of deviations from a prescribed parallel flow. If we let u, w denote streamwise and wall-normal velocity components corresponding to a two-dimensional perturbation from the parallel flow $\mathbf{U} = (U_p(z), 0, 0)$, and let ω denote the associated vorticity perturbation, then the Navier–Stokes equations can be cast in the form

$$\frac{\partial \omega}{\partial t} + U_p \frac{\partial \omega}{\partial x} + \frac{\partial (u\omega)}{\partial x} + \frac{\partial (w\omega)}{\partial z} + wU_p'' = \frac{1}{R}\nabla^2 \omega + \frac{1}{R}U_p''',$$

$$\nabla^2 w = -\frac{\partial \omega}{\partial x},$$

$$u = -\int_z^\infty \left(\omega + \frac{\partial w}{\partial x}\right) dz,$$

where ∇^2 now denotes the two-dimensional Laplacian.

It may be seen that, just as for the three-dimensional formulation, the streamwise perturbation velocity component u is defined explicitly in terms of the wall-normal component w and the vorticity perturbation ω. Thus, u may be eliminated from the vorticity transport equation, leaving a system of two partial differential equations for the two unknowns ω, w. It should also be noted that the profile $U_p(z)$ of the parallel flow may be chosen to take any form that is convenient for the problem at hand: it certainly does not need to be an exact solution of the Navier–Stokes equations. Parallelized simulations can be conducted by simply omitting the final term $1/RU_p'''$ from the right-hand side of the transport equation. This term would otherwise act as a source for the generation of a nonparallel base flow.

We suppose that the boundary conditions at the location $z = \eta(x, t)$ of the solid surface bounding the flow take the form

$$u(x, \eta, t) = u_w(x, t), \quad w(x, \eta, t) = w_w(x, t).$$

The integral condition that constrains the evolution of the vorticity is then given by

$$\int_\eta^\infty \omega \, dz = -u_w - \int_\eta^\infty \frac{\partial w}{\partial x} \, dz.$$

As before, this is fully equivalent to the no-slip condition. Continuity holds at all locations provided only that the normal-velocity satisfies the condition

$$\frac{\partial w}{\partial z} \to 0 \quad \text{for } z \to \infty.$$

As was mentioned briefly in the main text, the two-dimensional formulation has also been employed to compute the steady flow near the trailing edge of a flat plate. Essentially, all that was required was that the vorticity integral condition be exchanged for the simple center-line symmetry condition

$$\omega(x, 0, t) = -U_p'(0),$$

for locations in the wake beyond the end of the plate.

Finally, we remark that some of the ideas that we developed within our velocity–vorticity formulation could also find an application in a streamfunction–vorticity formulation for the case of two-dimensional flow. In particular, if we introduce a streamfunction ψ, then the no-slip condition can be very simply translated into a vorticity integral constraint of the form

$$\int_\eta^\infty \omega \, dz = -u_w + \int_\eta^\infty \frac{\partial^2 \psi}{\partial x^2} \, dz.$$

Coupling the enforcement of this condition to the solution of the vorticity transport equation provides a rigorous alternative to the employment of an artificial wall-vorticity boundary condition.

ACKNOWLEDGMENTS

The research described in this paper was carried out in part with the support of the Engineering and Physical Sciences Research Council.

REFERENCES

1. P. Balakumar and M. R. Malik, Traveling disturbances in rotating-disk flow, *Theoret. Comput. Fluid Dyn.* **2**, 125 (1990).
2. K. E. Barrett, A variational principle for the stream function-vorticity formulation of the Navier–Stokes equations incorporating no-slip conditions, *J. Comput. Phys.* **26**, 153 (1978).
3. F. Bertagnolio and O. Daube, Solution of the div-curl problem in generalized curvilinear coordinates, *J. Comput. Phys.* **138**, 121 (1997).
4. F. P. Bertolotti, Th. Herbert, and P. R. Spalart, Linear and nonlinear stability of the Blasius boundary layer, *J. Fluid Mech.* **242**, 441 (1992).
5. V. Bojarevics, G. Tinios, K. Pericleous, and M. Cross, CFD modelling of magnetic levitation casting. In *Proc. Int. Cong. Electromagnetic Processing of Materials.* (Centre Français de l'Electricité, 1997), Vol. 2, pp. 211–216.
6. C. Canuto, M. Y. Hussaini, A. Quarteroni, and T. A. Zang, *Spectral Methods in Fluid Dynamics* (Springer-Verlag, Berlin/NewYork, 1988).
7. A. Campion-Renson and M. J. Crochet, On the stream function-vorticity finite element solution of Navier–Stokes equations, *Int. J. Num. Meth. Eng.* **12**, 1809 (1978).
8. H. A. Carlson and J. L. Lumley, Active control in the turbulent wall layer of a minimal flow unit, *J. Fluid Mech.* **329**, 341 (1996).
9. H. A. Carlson and J. L. Lumley, Flow over an obstacle emerging from the wall of a channel, *AIAA J.* **34**, 924 (1996).

10. P. W. Carpenter, Status of transition delay using compliant walls, in *Viscous Drag Reduction in Boundary Layers* edited by D. M. Bushnell and J. N. Hefner, (AIAA Press, Washington, DC, 1990), pp. 79–113.
11. P. W. Carpenter, D. A. Lockerby, and C. Davies, *Numerical Simulation of the Interaction of MEMS Actuators and Boundary layers*, Technical Paper 2000–4330 (AIAA Press, Washington, DC, 2000).
12. A. J. Cooper and P. W. Carpenter, The stability of rotating-disc boundary-layer flow over a compliant wall, Part 1. Type I and II instabilities, *J. Fluid Mech.* **350**, 231 (1997).
13. O. Daube, Resolution of the 2D Navier–Stokes equations in velocity–vortcity form by means of an influence matrix technique, *J. Comput. Phys.* **103**, 402 (1992).
14. C. Davies and P. W. Carpenter, Numerical simulation of the evolution of Tollmien–Schlichting waves over finite compliant panels, *J. Fluid Mech.* **335**, 361 (1997).
15. C. Davies and P. W. Carpenter, Instabilities in a plane channel flow between compliant walls, *J. Fluid Mech.* **352**, 205 (1997).
16. C. Davies and P. W. Carpenter, A Novel Velocity–Vorticity Formulation of the Navier–Stokes Equations Part II: Global Behaviour Corresponding to the Absolute Instability of the Rotating-Disk Boundary Layer, Technical Report 2000/1 (Fluid Dynamics Research Centre, Univ. Warwick, 2000).
17. R. T. Davis, Numerical solution of the Navier–Stokes equations for symmetric laminar incompressible flow past a parabola, *J. Fluid Mech.* **51**, 417 (1972).
18. S. C. R. Dennis and J. D. Hudson, An h^4 accurate vorticity-velocity formulation for calculating flow past a cylinder, *Int. J. Num. Meth. in Fluids* **21**, 489 (1995).
19. S. C. R. Dennis and J. D. Hudson, Methods of solution of the velocity-vorticity formulation of the Navier–Stokes equations, *J. Comput. Phys.* **122**, 300 (1995).
20. D. C. R Dennis and L. Quartapelle, Some uses of Green's theorem in solving the Navier–Stokes equations, *Int. J. Numer. Meth. Fluids* **9**, 871 (1989).
21. H. Fasel, Investigation of the stability of boundary layers by a finite difference model of the Navier–Stokes equations, *J. Fluid Mech.* **78**, 355 (1976).
22. H. Fasel, Recent developments in the numerical solution to the Navier–Stokes and hydrodynamic stability problems, in *Computational Fluid Dynamics* (Hemisphere, 1980), pp. 167–280.
23. H. Fasel and U. Konzelmann, Non-parallel stability of a flat-plate boundary layers using the complete Navier–Stokes equations, *J. Fluid Mech.* **221**, 311 (1990).
24. H. Fasel, U. Rist, and U. Konzelmann, Numerical investigation of the three-dimensional development in boundary-layer transition, *AIAA J.* **28**, 29 (1990).
25. T. B. Gatski, Review of incompressible fluid flow computations using the vorticity–velocity formulation, *Applied Numer. Meth.* **7**, 227 (1991).
26. T. B. Gatski, C. E. Grosch, and M. E. Rose, A numerical study of the 2-dimensional Navier–Stokes equations in vorticity–velocity variables, *J. Comput. Phys.* **48**, 1 (1982).
27. T. B. Gatski, C. E. Grosch, and M. E. Rose, A numerical-solution of the Navier–Stokes equations for 3-dimensional, unsteady, incompressible flows by compact schemes, *J. Comput. Phys.* **82**, 298 (1989).
28. P. M. Gresho, Some interesting issues in incompressible fluid dynamics, both in the continuum and in numerical simulation, *Adv. Applied Mech.* **23**, 45 (1991).
29. P. M. Gresho, Incompressible fluid dynamics: some fundamental formulation issues, *Ann. Rev. Fluid Mech.* **23**, 413 (1991).
30. G. Guevremont, W. G. Habashi, and M. M. Hafez, Finite element solution of the Navier–Stokes equations by a velocity–vorticity method, *Int. J. Num. Meth. Fluids* **10**, 461 (1990).
31. Th. Herbert, Parabolized stability equations, *Ann. Rev. Fluid Mech.* **29**, 245 (1997).
32. L. M. Hofmann and Th. Herbert, Disturbances produced by motion of an actuator, *Phys. Fluids* **9**, 3727 (1997).
33. L. M. Hofmann and Th. Herbert, Reproducing the flow response to actuator motion, *J. Comput. Phys.* **142**, 264 (1998).
34. S. Houten, J. J. Healey, and C. Davies, Nonlinear evolution of Tollmien-Schlichting waves at finite Reynolds numbers, in *Proc. IUTAM Symp. on Laminar-Turbulent Transition, Sedona, USA*, edited by H. Fasel and W. S. Saric (Springer-Verlag, Berlin/New York, 1999).
35. C. E. Jobe and O. R. Burggraf, The numerical solution of the asymptotic equations of trailing edge flow, *Proc. Roy. Soc. London A* **340**, 91 (1974).

36. Th. von Kármán, Über laminare und turbulente Reibung. *Z. Angew. Math. Mech.* **1**, 233 (1921).
37. J. Kim, P. Moin, and R. Moser, Turbulence statistics in fully developed channel flow at low Reynolds number, *J. Fluid Mech.* **177**, 133 (1987).
38. L. Kleiser and T. Zang, Numerical simulation of transition in wall-bounded shear flows, *Ann. Rev. Fluid Mech.* **23**, 495 (1991).
39. M. Kloker, U. Konzelmann, and H. Fasel, Outflow boundary conditions for spatial Navier–Stokes simulations of transition boundary-layers, *AIAA J.* **31**, 620 (1993).
40. W. Koch, Direct resonance in Orr–Sommerfeld problems, *Acta Mechanica* **58**, 11 (1986).
41. Y. M. Koh and P. Bradshaw, Numerical solution of two-dimensional or axisymmetric incompressible flow using the vorticity equations, *KSME Journal* **8**, 264 (1994).
42. L. D. Kral and H. F. Fasel, Direct numerical-simulation of passive control of 3-dimensional phenomena in boundary-layer-transition using wall heating, *J. Fluid Mech.* **264**, 213 (1994).
43. R. J. Lingwood, Absolute instability of the boundary layer on a rotating disc, *J. Fluid Mech.* **299**, 17 (1995).
44. R. J. Lingwood, An experimental study of absolute instability of the rotating-disk boundary-layer flow, *J. Fluid Mech.* **314**, 373 (1996).
45. C. Liu and Z. Liu, High order finite difference and multigrid methods for spatially evolving instability in a planar channel, *J. Comput. Phys.* **106**, 92 (1993).
46. M. R. Malik, The neutral curve for stationary disturbances in rotating-disk flow, *J. Fluid Mech.* **164**, 275 (1986).
47. M. R. Malik and P. Balakumar, Nonparallel stability of rotating disk flow using PSE, in *Instability, Transition and Turbulence*, edited by M. Y. Hussaini, A. Kumar, and C. L. Streett (Springer-Verlag, Berlin/New York, 1992), pp. 168–180.
48. M. R. Malik, S. P. Wilkinson and S. A. Orszag, Instability and transition in rotating disk flow, *AIAA J.* **19**, 1131 (1981).
49. H. L. Meitz and H. F. Fasel, A compact-difference scheme for the Navier–Stokes equations in vorticity-velocity formulation, *J. Comput. Phys.* **157**, 371 (2000).
50. R. Rathnasingham and K. S. Breuer, Coupled fluid-structural characteristics of actuators for flow control, *AIAA J.* **35**, 832 (1997).
51. H. L. Reed and W. Saric, Stability of three-dimensional boundary layers, *Ann. Rev. Fluid Mech.* **21**, 235 (1989).
52. D. Rempfer and H. F. Fasel, Dynamics of 3-dimensional coherent structures in a flat-plate boundary-layer, *J. Fluid Mech.* **275**, 257 (1994).
53. D. Rempfer and H. F. Fasel, Evolution of 3-dimensional coherent structures in a flat-plate boundary-layer, *J. Fluid Mech.* **260**, 351 (1994).
54. U. Rist and H. Fasel, Direct numerical simulation of controlled transition in a flat-plate boundary layer, *J. Fluid Mech.* **298**, 211 (1995).
55. H. Schlichting, *Boundary-Layer Theory*, 7th ed. (McGraw-Hill, NewYork, 1979), pp. 102–104.
56. W. Z. Shen and T. Ph. Loc, Numerical method for unsteady 3D Navier–Stokes equations in velocity–vorticity form, *Comput. Fluids* **26**, 193 (1997).
57. C. G. Speziale, On the advantages of the vorticity velocity fomulation of the equations of fluid-dynamics, *J. Comput. Phys.* **73**, 476 (1987).
58. M. Turkyilmazoglu and J. S. B. Gajjar, *Absolute and Convective Instabilities in Incompressible Boundary Layer on a Rotating Disc*, Internal Report CLSCM-1998-002 (University of Manchester, 1998).
59. J. T. Trujillo and G. E. Kaniadakis, A penalty method for the vorticity-velocity formulation, *J. Comput. Phys.* **149**, 32 (1999).
60. E. Weinan and J. G. Liu, Vorticity boundary condition and related issues for finite difference schemes, *J. Comput. Phys.* **124**, 368 (1996).
61. X. H. Wu, J. Z. Wu, and J. M. Wu, Effective vorticity-velocity formulations for 3D incompressible viscous flows, *J. Comput. Phys.* **122**, 68 (1995).